X-661-72-316
PREPRINT

NASA TM X- 66037

ENERGY CALIBRATION OF A COSMIC RAY IONIZATION SPECTROMETER

HAVEN WHITESIDE
CAROL JO CRANNELL
HALL CRANNELL
JONATHAN F. ORMES
MICHAEL J. RYAN
W. VERNON JONES

SEPTEMBER 1972

GODDARD SPACE FLIGHT CENTER
GREENBELT, MARYLAND

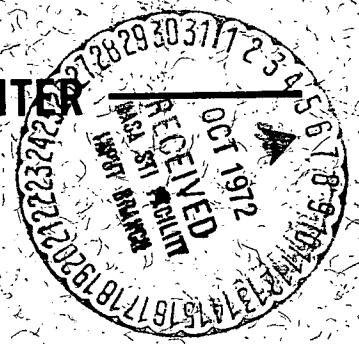

ENERGY CALIBRATION of a COSMIC RAY IONIZATION SPECTROMETER*

Haven Whiteside and Carol Jo Crannell
Department of Physics
Federal City College
Washington, D.C. 20005

and

Hall Crannell
Department of Physics
The Catholic University of America
Washington, D.C. 20017

and

Jonathan F. Ormes and Michael J. Ryan+
NASA/Goddard Space Flight Center
Greenbelt, Maryland 20771

and

W. Vernon Jones
Department of Physics and Astronomy
Louisiana State University
Baton Rouge, Louisiana 70803

* Work supported in part by NASA Grant NGR 09-005-007 and NGR 09-050-001
+ NAS/NRC Resident Research Associate; Present Address: 28 Wells Street, East Gosford, N.S.W. Australia 2250

ENERGY CALIBRATION OF A COSMIC RAY IONIZATION SPECTROMETER

Table of Contents

II

Abstract

The NASA/GSFC High Energy Cosmic Ray Experiment was calibrated at the AGS at Brookhaven National Laboratory during the summer of 1970 using protons and pions with energies from 9.3 GeV to 17.6 GeV.

The best measure found for the energy E of an incoming primary particle is ΣI, the total number of ionizing particles observed in the instrument, summed over the various iron modules. The resolution in the calibration energy range is about $\pm 30\%$ (s.d.) over a wide range of incident angles and positions.

The calibration function may be parameterized as $E = \Sigma\ I/K$, where K is predominantly a function of the location of the first interaction and the trajectory of the incoming particle. To a fair approximation the geometrical dependence of K can be encompassed by writing K as a function of d, the distance from the first interaction along the primary ray to the edge of the instrument. Empirically, $K = 5.83\ (1-\exp(-d/\lambda))\ \cos\theta$, where λ is a characteristic length which is a slowly varying function of energy. The value of K, and thus the average energy values calculated from the experimental data are accurate to about $\pm 10\%$ under calibration conditions.

Introduction

In a series of satellite flights, a group of scientists from the USSR has measured the spectrum of primary cosmic ray protons[1] and observed an unexpected bend in this spectrum. That is, they found that the exponent of the integral spectrum changes from 1.62 to 2.3 at a proton energy of 1000 GeV. This observation contradicts the predictions based on our current understanding of the origin of cosmic rays and it differs from the observed

spectrum of all cosmic ray particles over the same energy range. It is therefore important that these results be checked and that they be extended to include measurements of the spectra of other charge components individually. To accomplish these objectives an experiment is being prepared to be flown on the High Energy Astronomy Observatory in 1975. A prototype has been built and flown on balloons, with encouraging results at energies up to 2000 GeV.[2]

The type of instrument used to measure energy in both the USSR experiment and in this one is an ionization spectrometer or "calorimeter".[3] Since these devices are of finite thickness and sample only a fraction of the incident energy, it is exceedingly important to calibrate their response using incident beams of known energy. A test beam from the Alternating Gradient Synchrotron at Brookhaven National Laboratory was used in the calibration that is the subject of this paper. In order to extrapolate the response to higher energies a Monte Carlo simulation has been used, and this simulation is checked by comparison with the calibration data obtained at the A.G.S.

I. The Instrument

The prototype instrument[4] has been designed and built at Goddard Space Flight Center in order to study cosmic ray primaries in the energy range 10^{10} to 10^{12} eV. This instrument is intended to be carried to high altitude (38,000 m) by a research balloon, and it is designed to have an energy accuracy much improved over previously existing spectrometers.

This instrument contains four pairs of wire-grid spark chamber planes to define the trajectory of the incoming particle (see Figure I-1). It also contains a charge-determining module consisting of two plastic

scintillators and a CsI(Tℓ) scintillator with response functions proportional to Z^2/β^2, and a Cerenkov detector with an output proportional to $Z^2(1 - \frac{1}{\beta^2 n^2})$ where Z is the charge, β is the speed of the incident particle relative to the velocity of light and n is the index of refraction of the Lucite Cerenkov radiator. Together, these four detectors enable the determination of the charge of the incoming particles to within one unit of charge up to Z = 26. The two plastic scintillators also provide triggers for the spark chamber system.

For energy measurement, an ionization spectrometer (IS) is used. This instrument consists of alternate layers of high-Z absorber and plastic scintillator. Each scintillator section is viewed by a pair of photo-multiplier tubes, the outputs of which are proportional to the number of ionizing particles traversing that section of the spectrometer. The cascade shower induced by the incoming particle results in many secondary particles. Measurement of the number of secondary particles at many points in the shower enables reconstruction of the shower curve and determination of the energy of the incident particle. The top abosrber layers are made of tungsten, which rapidly develops electromagnetic cascade showers, producing a distinct signature for incident electrons. The lower layers are made of iron to study incoming nucleons and nuclei by means of their nuclear cascade showers.

Each iron module consists of .75 radiation lengths (r.l.) of iron, a 1/4" thick Pilot Y scintillator, 1.5 r.l. of iron, another scintillator, another 1.5 r.l. of iron, a third scintillator, and finally .75 r.l. of iron. The light from the three scintillators is summed by coupling to a single pair of photomultiplier tubes for each module. Because the energy measured is primarily that which has found its way into electromagnetic cascades through π° decay, 1.5 radiation lengths is an appropriate interval for sampling

the energy.

Each iron module is also approximately 0.5 nuclear interaction lengths thick, and the complete spectrometer contains seven modules or 3.5 nuclear interaction lengths of iron, with the pulse heights recorded separately for each of the seven modules. This allows location of the first interaction within half an interaction length.

The electron section contains 12 tungsten modules, each 1 radiation length thick, containing a sheet of tungsten and a single plastic scintillator, viewed by a pair of photomultiplier tubes. The entire electron section is 0.44 nuclear interaction lengths thick.

The ionization spectrometer weighs 2.5 tons. For flight purposes it is contained in a gondola 1.5 m in diameter by 2.5 m long. The geometry factor for particles that traverse at least 3 mfp of material is about 495 cm^2-sr. The electronics readout time (dead time) averages 0.06 sec per event, but the detector remains active for only 2 microseconds after passage of the incident particle. The internal layout is shown in schematic form in Fig. I-1. A photograph of the entire instrument, with the cover removed, is shown in Fig. I-2.

II. Experimental Calibration

In order to use the IS to measure particle energies above accelerator energies, it is necessary to make a theoretical analysis of detector response as a function of energy. The response, however, is also a function of arrival direction and particle type. The theoretical analyses for a variety of experimental parameters are greatly facilitated by the use of Monte Carlo techniques. A Monte Carlo computer program has been developed

by W. V. Jones[5] and employed in the present work. Predictions based on the same program are being employed in the design of the IS for the HEAO-A satellite experiment.

However, in order to make absolute energy measurements, the IS response must be calibrated using particles of known energy. This is necessary in order to verify the applicability of the assumptions on which the calculations are predicated as well as to measure the efficiency of various components in the system. Also, since the energy of each incoming particle is only sampled by the detector, the accuracy and the resolution of these measurements depend on the fluctuations in the energy contained and energy lost by the IS. The distribution of these fluctuations must also be studied in the calibration run.

Since the instrument is designed for energy measurements in the range 10^{10} to 10^{12} eV, this calibration has been performed at the highest machine energy available at this time. The data for this purpose were obtained using a proton or pion beam at the Alternating Gradient Synchrotron at Brookhaven National Laboratory, in a manner similar to that used by a group from Max Planck Institute and Louisiana State University with an earlier instrument.[6] Lower energies were also used in order to allow a good check of the theory which is to be used to extrapolate to even higher energies. Because the fraction of the incident energy which escapes from the detector depends on the angle of incidence and the transverse position, the calibration has been carried out at several different angles and beam positions. Calibration of the electron section has previously been accomplished using 5.4 to 18 GeV electrons at SLAC.[7] Calibration of the nuclear section is the subject of this report.

The experiment was set up in the G-10 + 4.7° Test Beam[8] in the East Experimental Area at the AGS. The configuration of the beam transport system is given in Table II-1 and illustrated in Fig. II-1. Because of power supply limitations, the maximum available momentum was about 20 GeV/c. Of the quadrupoles, only Q_5 and Q_6 were available during these runs, since power limitations prevented the use of Q_2, and the power supplies for the other quadrupoles had been removed. Details of the experimental set-up have been given in an earlier report.[9]

The IS was supported in a horizontal position by jackscrews on a wheeled cart, as shown in Fig. II-2, allowing the horizontal position and orientation as well as the vertical position to be changed with respect to the incoming beam. The whole experiment was encased in a large light-tight tent to prevent light leakage into the photomultiplier tubes.

Twenty-three production runs of one to five thousand events each were made, as listed in Table II-2. These runs allow the study of the dependence of detector response on:

(1) Energy (from 9.3 to 17.6 GeV)

(2) Angle of Incidence (from 0° to about 20°)

(3) Position of Incident Particle (various locations over the aperture)

(4) Incident Particle (protons and pions)

(5) Depth of Spectrometer (up to 4 nuclear interaction lengths).

III. Response of the Detector

Perhaps the most revealing measures of detector response for an ionization spectrometer are the mean shower curves measured for various beam energies, positions and angles of incidence. These curves are easily

measured and are directly related to the physical processes in shower development. They are also convenient to compare with the predicted curves obtained from a Monte Carlo analysis of the detector. Comparisons for several typical runs are shown in Figs. III-1 through III-6. For the data presented in these figures, the particular events chosen are those for which the first interaction takes place in the first iron module or the last tungsten module, according to the interaction definition described below.

The shower curves show the number of equivalent particles observed traversing each module of the detector, where one equivalent particle produces a pulse height equal to that of one muon as described in the section on Normalization, below. The error bars show the standard deviation of the mean for the mean number of particles observed in each detector. It can be seen that agreement is qualitatively quite good between the experimental data and the Monte Carlo prediction. This agreement is important since it confirms the Monte Carlo model which will be used to extrapolate the spectrometer response to energies beyond the range of machine calibration.

The mean value of χ^2 for these curves is two or three times the value expected from statistical consideration so that the difference between experimental results and predictions of the Monte Carlo model cannot be attributed to statistical fluctuations alone. However, considering the complexity of the processes involved, differences of this size are probably reasonable. The discrepancy suggests, however, that the uncertainty in extrapolations made by using the Monte Carlo model may be as much as twice the uncertainty due to statistical considerations. The shape of the mean shower curves is also quite interesting. The shower develops rapidly,

reaching a maximum within one iron module (approximately 4.5 rl) of the first interaction. Then it decays in exponential fashion, with a characteristic length λ of 2.2 $\pm$0.1 module. Since each module contains 66.4 g/cm^2 of iron and 1.95 g/cm^2 of Pilot Y (4.6 g/cm^2 iron equivalent), one module is equivalent to 71.0 g/cm^2 of iron. Therefore, the decay length of the mean shower curve in iron is 156 g/cm^2 at these energies, a value which lies between the proton and pion interaction lengths in iron.[10]

In the calibration of the detector it is important to analyze the event-by-event fluctuations as well as the mean response, since these fluctuations are quite large and will ultimately limit the resolution. For example, Fig. III-7 shows a histogram of the number of particles observed in the second iron module for events interacting in either the last tungsten or the first iron module. This detector is located at the mean shower maximum for these events. In this instance, fluctuations are of the order of $\pm$50% of the mean, with a few events up as high as 150% above the mean. The asymmetry of the curve comes from the fact that the probability distribution for energy loss by a singly charged particle follows a distribution which has a long tail extending to large energy losses. Physically this is due to fluctuations in multiplicity, in elasticity, and electron shower development.

Here it is seen that the shape of the distribution from the Monte Carlo calculation is slightly different from that obtained experimentally in that the M-C calculation peaks at a lower number of equivalent particles and has a somewhat longer tail. Despite this difference the mean values and the widths of the two histograms agree reasonably well, within about 10%.

Fig. III-8 shows a histogram of the sum of the number of particles observed in all seven iron modules. It is clear that the agreement between the mean values from the experiment and the Monte Carlo calculation is much better for this sum than it is for the signal observed in a single module. This agreement is encouraging, because it is this sum, rather than any individual signal, that will be used as a measure of the energy. However, it should be noted that the Monte Carlo calculation gives a slightly narrower distribution than that observed experimentally (standard deviation 17% compared to 21%). This is probably due to the many instrumental sources of fluctuations in the actual measurements in addition to the physical sources of fluctuations included in the Monte Carlo Model.

A second quantity that could have been used as a measure of the energy of the incoming particle is the number of particles at shower maximum. The histogram in Fig. III-9 shows that this gives a standard deviation of +36%, -31%, using the experimental data. However, the total number of particles in 7 iron modules gives much better resolution ($\pm$21%) and is therefore the preferred measure of energy. This result is confirmed at other angles and other energies.

IV. Geometrical Considerations

A. Detector Response Factor

The detector response depends on various geometrical factors such as the position and angle of the trajectory of the incident particles as well as the location of the first interaction. One of the major purposes of this

calibration was to explore this dependence. For this purpose it is convenient to define a detector response factor K, which is simply the ratio of the total number of equivalent particles observed in all the iron modules ΣI to the energy E of the incident primary particle

$$K = \frac{\Sigma I}{E} \qquad (1)$$

B. Depth Dependence

A study of the dependence of K upon the residual path from the point of the first interaction to the exit point of the primary ray (see Fig. IV-1) shows that it asymptotically approaches a maximum as the residual path increases. This is to be expected since the shower generally reaches its maximum within one iron module from the first interaction point and dies out thereafter (see Figs. III-1 through III-6). As the residual path increases a larger and larger fraction of the shower is contained within the instrument.

An expression for the response factor can be derived from the mean shower curve by noting that the mean shower curve resembles a decaying exponential, proportional to $\exp(-S/\lambda)$ where S is distance along the particle path. Since the total number of particles observed in the spectrometer equals the integral of the shower curve from the interaction point to the bottom of the detector (for particles incident at 0° on the center of the instrument) we find that ΣI is proportional to $[1 - \exp(-d/\lambda)]$, where d is the residual path from the interaction point to the exit point, and $\lambda = 2.2 \pm 0.1$ module from the mean shower curves themselves. Hopefully, the proportionality constant itself will not be energy dependent. (This is discussed below in Section IX). Choosing this constant empirically for best fit at large d

we find (for $\theta = 0$)

$$K = 5.83\ [1 - \exp\ (-d/\lambda)]. \qquad (2)$$

The predictions of Eq. 2 are compared with the experimental and Monte-Carlo results in Fig. IV-1. Agreement is seen to be excellent, except at small d. For small d Eq. 2 predicts values of K that are larger than those observed. This behavior is to be expected because the mean shower curve lies below a true exponential at points before shower maximum. Therefore events with a residual path of less than 20 cm (1 nuclear interaction length) are not used in the analysis, since they will given an unreliable estimate of the energy.

The detector resolution is also dependent on the residual path, as shown in Fig. IV-2. The resolution improves with increasing path lengths, approaching a value that is in the neighborhood of 20%. The measure used for this resolution is the percent standard deviation of the total number of equivalent particles observed in the iron modules, ΣI Since ΣI exhibits the usual statistical fluctuations associated with nuclear processes, (see Fig. III-8) and ΣI itself increases with increasing residual path this effect is reasonable. It is also noted that the experimental resolution is not quite as good as the Monte Carlo predictions. This was discussed in Sec. III.

C. Angular Dependence

A study of the dependence of K upon the angle θ between the trajectory of the incident particle and the axis of the instrument shows a significant decrease in K as the angle is increased (Fig. IV-3). This is to be expected for particles traveling at moderate or large angles since some fraction of the shower will exit through the side of the instrument before it dies out and thus some shower particles are lost.

The expected value of K can be estimated by considering the residual path d from the point of interaction to the point where the shower axis leaves the instrument as shown in Fig. IV-4. For the calibration runs we use a mean value for d, averaged over the beam width.

Assume that the beam enters the apparatus and passes through the spark chamber (S.C. at z = 0 and x = x and at an angle θ with respect to the spectrometer axis. It interacts at point P and then would exit at point E if it continued. From geometrical considerations we find that $z_E = -x/\tan\theta$ while $z_p = -40.5$ cm for interactions in the first iron module, etc. Also,

$$d = \frac{z_p - z_E}{\cos\theta} \tag{3}$$

and then it is possible to calculate an expected value for K using Eq. 2 above. There is however one more correction to be made: the raw-value of ΣI represents the number of equivalent particles observed. But, when the particles travel at an angle to the axis, each particle deposits more energy per module because it has a longer path in each module. To take this effect into account it is necessary to multiply by cos θ to get the correct value for K (recall that ΣI is divided by K to give the measured energy). Thus

$$K = 5.83\ (1 - \exp(-d/\lambda))\ (\cos\theta). \tag{4}$$

Figure IV-3 shows the dependence of the detector response upon angle at two different energies. The error bars (size of the circles for Monte Carlo predictions) indicate the standard deviation of the mean value of K at each point. It is seen that the experimental results are approximated surprisingly well by Eq. 4. The Monte Carlo predictions also agree very well at 17.6 GeV except at 20° although they give values that are consistently a bit low at 9.3 GeV. The reason for the discrepancy at 17.6 GeV, 20° is that the Monte

Carlo events were farther from the edge of the instrument than the experimental events, as discussed below in Sec. V.

D. Position Dependence

A study of the dependence of K upon the position of the incident beam (at 0° angle) shows a drop in K as the beam approaches the side of the detector (see Fig. IV-5). This behavior occurs because part of each shower will be lost out the side. Statistics are not very good on these data, but the smooth curves which have been interpolated between data points allow one useful conclusion to be drawn. Detector response is at least 90% of its central value for beams which lie at least 6 cm from the edge of the detector. This suggests that events whose trajectory lies nearer to the side of the detector that 6 cm should not be considered in any experimental sample, since they will give an unreliable estimate of the energy. Alternatively, a correction could be applied to take side losses into account. This was not done because its complexity and the small number of events involved.

The Monte Carlo predictions which are also shown in Fig. IV-5 agree with experiment exceedingly well at 9.3 GeV and at 17.6 GeV.

V. Pulse Height Normalization

The outputs from each detector are normalized in terms of the pulse heights produced by a standard equivalent particle. The standard particles used were several hundred non-stopping muons accumulated with the AGS off. The normalization factors for odd-numbered detectors were obtained by requiring that the pulse heights in all even-numbered detectors fall in a range characteristic of the passage of a single particle, and vice versa for the even-numbered detectors.

After the calibration runs, about 3500 muons were accumulated during several hours running with the AGS off, while the instrument was still in position. By analyzing these in a manner similar to protons it was possible to select unambiguously 2000 muons that stopped in a given detector, from I4 on. This defined their ranges, and allowed the incident energies and the energy losses in earlier detectors to be taken from the tables of Barkas & Berger.[11] This analysis showed that the energy loss of a standard equivalent particle is $1.56 \pm .07$ MeV/g/cm^2 in iron, equal to the energy loss of a 700 MeV muon and slightly above the minimum ionization value of 1.48 MeV/g/cm^2. As a result, a unit equivalent particle corresponds to an energy loss of $104/\cos\theta$ MeV/module.

VI. Interaction Definition

In order to locate the interaction which initiates a nuclear cascade one must first decide on a specific definition of an interaction. The definition used requires 3 or more particles to be observed in each of two consecutive iron modules, in which case the interaction is said to have taken place in the first of these iron modules. This definition includes all except a class of events for which the interaction has low charged pion multiplicity. Since our purpose is ultimately to determine the energy of the incoming primary, neglecting these events is insignificant because they represent only a small fraction of that energy.

This particular definition was chosen in connection with another analysis using this same data.[10] In that experiment the number of particles required in each module and the number of consecutive modules required to define an interaction were varied. The definition selected for the present analysis was that which gave the greatest statistical accuracy to the

interaction length measurement.

The number of interactions versus depth is shown in Fig. VI-1. It is seen that these follow an exponential law, consistent with an interaction length of 143 g/cm^2.

VII. Interactions in Tungsten

Approximately 40% of all incoming protons interact in the tungsten section of the spectrometer. Analysis of these events is complicated by the differences between the critical energies and radiation lengths in tungsten and in iron and the consequent transition effect in passing from one material to the other. Comparison with Monte Carlo-produced events suggests that the definition of the interaction point in tungsten should be different from that in iron. This is due mainly to the fact that the number of secondary particles produced in tungsten is approximately three times that produced in a similar thickness of iron because the electromagnetic cascade develops more rapidly in tungsten.

An example of 17.6 GeV protons interacting in a tungsten module is shown in Fig. VII-1. Note that the shower in tungsten is similar to that produced by a 4-GeV electron (or gamma ray or neutral pion). This similarity can produce some difficulties if one is trying to identify electrons in the presence of a high background of protons as is done in some cosmic ray experiments. Table VII-1 shows the total number of equivalent particles produced in iron and tungsten for four different interaction depths. The fraction of the energy deposited in the tungsten is very sensitive to the depth of interaction. It is difficult to predict how this fraction will vary with energy, but it should decrease with increasing primary energy because high energy nuclear cascade take longer to develop than low energy cascades.

VIII. Energy Dependence of Detector Response

The most useful result of this calibration is a curve of detector response as a function of primary energy. It is this curve that enables the analysis of the energy of incident cosmic rays, since the curve shows how to calculate the (unknown) primary energy from the observed signal (ΣI). Figure VIII-1 shows these curves for three different angles of incidence. One expects a linear dependence, and straight lines have been drawn through the experimental points. It is also expected that these straight lines should pass near the origin, since a zero energy primary should produce zero secondary particles. This appears to hold only very roughly, especially for angles of 14° and 20°.

The Monte Carlo results are plotted on the same coordinates, and agreement is seen to be excellent at 0°. At larger angles the Monte Carlo results differ significantly from the measured values. The difference is greatest at 20°, where the experimental results lie below the Monte Carlo predictions. This may be partially explained by the fact that the experimental events which satisfied the interaction criteria used here were not centered on the instrument, but were displaced 2 to 8 cm towards the edge, thus reducing the path of the shower within the instrument. Also, the distribution of particles across the beam, both in area and in angle is not quite the same for the experiment as for the Monte Carlo model, and this may cause some differences in the results, especially at angles off the axis.

Figure VIII-2 shows the detector response calculated from the Monte Carlo events at 0° incidence which interact in the first iron module, over an energy range extending from 10 to 1000 GeV. Within a few percent, the response is linear over this entire range, corresponding to a response factor $K = 5.54$.

IX. Detector Response Function

The above analysis shows how the average detector response varies as a function of various parameters. Using these experimental data, it is possible to interpolate and/or extrapolate over a fairly wide range of situations. In analyzing an actual cosmic ray experiment one can select certain events, for example: events with interactions early in the iron, and trajectories making small angles with the axis and not too near the sides of the spectrometer. For such events it is po-sible (see Fig. VIII-1) to assume that ΣI is directly proportional to primary energy, and the proportionality constant can be obtained from the calibration data. The energy spectrum is then easily obtained using the relation

$$E = \frac{\Sigma I}{K} , \qquad (5)$$

where E is in GeV, ΣI is in number of equivalent particles, and K = 5.56 for interactions in the first iron module.

This method, although accurate, suffers from one major disadvantage: events which do not satisfy these rather strict criteria are rejected so that the statistical significance of the experiment is less than it might be. For certain measurements, especially those of rare types of particles such as heavy nuclei, it will be important to analyze as many events as possible. Unfortunately, the actual response observed in any given event depends on many parameters and also is subject to large fluctuations so that the analysis could become too complicated to execute efficiently.

One possible approach to this problem is to use less stringent criteria on the interaction point, etc. However, when this is done, the fact that a single value of K is used over a wide range of situations causes a significant loss in resolution. Another method of analysis is to assume

the detector response factor K previously defined in Eq. 1 to be a function only of d, the residual path from the point of interaction to the boundary of the instrument, and E, the energy of the incoming primary. The dependence on d incorporates all the dependence on angle, position and depth. The dependence on E comes about because the unobserved fraction of the primary energy which goes into nuclear disintegrations decreases as E increases. Also the decay length of the mean shower curve increases as energy increases, partly due to the decrease in nuclear cross sections with increasing energy.[12]

The previous analysis leading to Eq. (4) suggests the form of K:

$$K\ (d,\ E) = K_o\ (1 - \exp\ (-d/\lambda))\ \cos\ \theta \qquad (6)$$

In the present calculation we have used constant values of $K_o = 5.83$ particles GeV^{-1} and $\lambda = 22$ cm, which are averages taken from the experimental mean shower curves at 9.3 and 17.6 GeV. For use over a wider energy range it is necessary to determine the functional dependence of K_o and λ upon the energy. The Monte Carlo data suggests the following empirical functions for use in the energy range 10-1000 GeV:

$$\lambda = (8.00 + 12.6\ \log_{10}\ E)\ \text{cm} \qquad (7)$$

$$K_o = (5.07 + 0.83\ \log_{10}\ (E-7))\ \text{particles GeV}^{-1}. \qquad (8)$$

Interestingly, the effects of the energy dependence of these two parameters tend to cancel each other out, and, for events with 0° angle of incidence and the first interaction in I1, K is essentially constant independent of energy. This is the reason for the linearity of the detector response as previously noted from Fig. VIII-2.

The experimental data do not cover a wide enough range of energies to test this function adequately; however they are consistent with it.

Now K and E can be calculated for each incoming event, and the only events which need be rejected are those which have residual paths less than some cutoff value. Studies of the effect of the cutoff show that it is not very sensitive to the choice of the cutoff value: for example, the calculated energy of a 17.6 GeV incoming beam at 14° to the axis only varies by 6% when the cutoff value of d is varied from 10 to 50 cm. A choice of 20 cm is convenient, and this ensures that in most cases shower maximum is reached before the shower exits from the instrument.

Table IX-1 shows a comparison between the actual energy and the calculated energy for three different methods of calculation, for a variety of beam conditions. Table IX-2 compares the accuracy of the three methods for events of the most likely geometry (0° to 14° angle of incidence, position at or near the center of the aperture). Method 1 uses all interactions in modules T12 through I6 and a constant value for K. Method 2 uses only interactions in module T12 or I1 and a (different) constant value of K. Method 3 again uses all interactions in modules T12 through I6, but with the response function K (d, E) as in Eq. (4).

Notice that method 1 gives the most events, method 2 gives the best resolution, and method 3 gives the best accuracy of energy determination. However, from Table IX-1 it is seen that Method 1 is so inaccurate for events at steep angles or near the edge that it must be ruled out for practical use. It is then clear that Methods 2 and 3 do not differ greatly in either accuracy or resolution, and that Method 3 is a significant improvement over Method 2 in the total number of events analyzed.

Conclusion

The calibration described here was designed to study the spectrometer response to protons of known energies and incident angles in order to predict the response to cosmic ray protons of energies as great as 1000 GeV. A detector response function was developed from the experimental data which enables satisfactory energy resolution (~30% s.d.) to be obtained for angles of incidence up to 14° and effective spectrometer depths as small as 3.5 interaction lengths.

On the basis of the Monte Carlo results the detector response function has been improved by including the energy dependence of its parameters. The resulting function agrees with the Monte Carlo results within a few percent over the entire range of 10-1000 GeV. It also agrees with the experimental results reported here, but a full experimental test must await a calibration at higher energies, possibly at NAL. The use of this improved detector response function will enable a determination of the cosmic ray proton flux with improved statistical accuracy from our current balloon flight data.

Acknowledgements

Thanks are extended to R. Lanou and L. Rosenson of the MIT-Brown Group for the use of the Cerenkov counter, and S. Siegler for the use of the beam telescope. We especially want to thank R. Kurz for providing us with the very useful report[13] of his BNL calibration. Thanks are also extended to J. Tanguay[14] and the entire crew at the AGS, who assisted in many ways. Appreciation is also expressed to the several other experimenters with whom we shared the Test Beam.

Several students participated in the data runs in addition to the authors of this report. These include: R. Silverberg of Goddard Space Flight Center, A. Peterson and D. Dellatorre of Catholic University of America, and R. Cunningham, J. Reynolds, and S. Withers of Federal City College.

Finally, a special word of appreciation is in order for the technical staff from Goddard Space Flight Center, including L. Stonebraker, J. Laws, M. Powers, and R. Greer, all of whom put in many long hours ensuring that the experiment would operate properly.

References

(1) V. V. Akimov, N. L. Grigorov, V. E. Nesterov, I. D. Rapoport, I. A. Savenko, G. A. Slairidin, and A. F. Titenkov, Proc. 11th Int. Conf. on Cosmic Rays, Acta Physica, Suppl. 1, 29, 517 (1970).

(2) M. J. Ryan, J. F. Ormes, and V. K. Balasubrahmanyan, Phys. Rev. Lett., 28, 985 (1972).

(3) V. S. Murzin in Progress in Elementary Particles and Cosmic Ray Physics Vol. 9, J. G. Wilson and S. A. Wouthuysen ed. (North-Holland, Amsterdam, 1971).

(4) J. F. Ormes, V. K. Balasubrahmanyan, F. B. McDonald and R. D. Price, IEEE Trans. Nucl. Sci., NS-15, 3, 566 (1968)

(5) W. V. Jones, Phys. Rev., 187, 1868 (1969)

(6) W. V. Jones, K. Pinkau, U. Pollvogt and W. K. H. Schmidt, Nucl. Inst. and Methods, 72, 173 (1969).

(7) C. J. Crannell, R. Gearhart, F. A. Hagen, W. V. Jones, R. J. Kurz, J. F. Ormes, R. D. Price, R. F. Silverberg and Y. M. Simnett, Electron Calibration of a High-Energy Cosmic Ray Detector, to be published.

(8) A. L. Read, Brookhaven National Laboratory E. P&S Div. No. 2, March 10, 1967.

(9) H. Whiteside, C. J. Crannell, H. Crannell, J. F. Ormes, and M. J. Ryan, Calibration of the NASA/GSFC High Energy Cosmic Ray Experiment, GSFC Technical Report X-661-71-36 (January 1971).

(10) H. Crannell, C. J. Crannell, H. Whiteside, J. F. Ormes, and M. J. Ryan, The Interaction Length of Energetic Pions and Protons in Iron, to be published.

(11) W. H. Barkas and M. J. Berger, Tables of Energy Losses and Ranges of Heavy Charged Particles, NASA SP-3013 (1964).

(12) W. V. Jones, Proc. 11th Int. Conf. on Cosmic Rays, Acta Physica, Suppl. (1970).

(13) R. J. Kurz, CRISP Calibration Experiment, NASA/MSFC Tech. Note 33, (1970).

(14) G. E. Tanguay, Brookhaven National Laboratory E P&S Div., Tech. Note No. 22, December 16, 1968.

List of Tables

TABLE II-I

LAYOUT OF G-10 + 4.7° TEST BEAM, 18-21 July, 1970

Element	Symbol	Location	Description
G-10 Target	T	Between G-10 & G-11 ring magnets	BeO wire, described in Reference (14)
Virtual Target	T_V	On a radial line through G10 target	BeO wire, offset by fringe field of G11
Collimator #1	C_1	268.25" from T	1" hor x 4" vert x 36" lead
Quadrupole #5	Q_5	563" from T on "magnet axis"	Type 8Q48
Quadrupole #6	Q_6	623" from T on "magnet axis"	Type 8Q48
Bending Magnet #1	D_1	701" from T	Type 18D72 - bend angle 3.4025° w.r.t. "magnet axis"
Collimator #2	C_2	460.75" from D_1	1/2" x 1/2" x 48" lead, with brass shims
Collimator #3	C_3	535.75" from D_1	Variable width x 4" vert. x 48" lead automatic collimator
Bending Magnet #2	D_2	950.5" from D_1	Type 18D72 - bend angle 1.3916°
Scint. Counter #1	S_1	500" from D_2 (Nominal)	4" wide x 3-1/2" high plastic
Cerenkov Counter	C	549" from D_2 (to entrance)	2 meter long gas Cerenkov counter
Scint. Counter #2	S_2	612" from S_1	1" x 1" plastic
Scint. Counter #3	S_3	55" from S_2	2" x 2" plastic
NASA Experiment	IS	2258" from D_2	Ionization Spectrometer

TABLE II-2

Calibration Runs

Tape	File	Number of Single Events	Particle	Energy (GeV)	Angle(°)	Position (in)* $\bar{x}$	Position (in)* $\bar{y}$	Position # and Comments
1	9	2871	p	13.85	13.8	8.6	9.2	1
	10	3631	p	13.85	2.3	10	9.4	1
	11	2822	p	17.8	14.3	8.4	8.8	1
	12	1184	p	9.4	13.8	8.6	9.4	1
	14	3265	p	9.3	21.8	9.0	9.4	1
	15	3548	p	9.3	28.7	14.6	9.4	5
	16	4411	p	9.3	2.3	11	9.6	1
	17	4368	π^+	9.3	1.8	10.2	9.5	1
	18	4342	p	9.3	2.3	10.2	13	2
	19	4551	p	9.3	2.3	10.0	16.6	3
	20	3664	p	9.3	1.7	2.6	16.6	4
	21	4342	p	17.6	2.3	1.9	16.4	4
	22	4057	p	17.65	2.9	8.2	16.8	3
2	2	2933	p	17.65	2.9	8.2	13.6	2
	3	2286	p	17.65	2	8.2	9.2	1
	4	952	p	17.65	2	8.2	9.2	1
	5	3827	p	17.6	1.2	7.9	8.7	1 (4 extra iron modules for these runs)
	6	4191	p	17.65	1.2	8.5	8.6	1
	7	2243	p	17.65	19.2	~13	9	Neck
	8	4824	p	17.65	18.4	7.2	8.6	1
	9	1189	π^+	17.65	1.5	7.8	9.0	1
	10	427	π^+	17.65	1.7	8.1	8.8	1
3	1-5	3589	μ	-	-	-	-	Cosmic Ray Muons

*Positions given are for the center of the beam. Typically 87% of the incident particles were within 2" radius of beam center. The center of the aperture of the instrument is at x=10, y=10 inches.

Table VII-1 Interactions in Tungsten

17.6 GeV, 0°, central position

Interaction Region	No. of Events	ΣT (1-12)	ΣI (1-7)	Energy in Tungsten
CsI - T3	313	370	62	35%
T4 - T7	219	215	79	18%
T8 - T11	255	62	95	2%
T12 - I1	362	16	97	1%

This run included 2047 simple events which satisfied geometrical criteria. In addition to the events tested above, there were 45 interactions in S_1, S_2 or the Cerenkov, 761 interactions in I 2-6 and 92 particles that did not interact before I 7.

Energy in tungsten is the fraction of the energy deposited in the spectrometer which produces the pulses in the tungsten portion.

TABLE IX-I COMPARISON BETWEEN ACTUAL AND CALCULATED ENERGY

1) All simple events K = 3.71
2) Simple Events, interact in T12 or I1 $6 < x,y < 14$ in, $0 < \theta < 1$ rad K = 5.07
3) Simple Events, interact in I1-I6 all x,y; $0<\theta<1$ rad; d>20cm

Tape/File	Angle	Position	E_{true}	E_1	E_2	E_3	σ_1	σ_2	σ_3	N_1	N_2	N_3
1/16	0°	1	9.3	10.5	10.3	9.3	48%	26%	28%	4175	588	1684
1/10			13.85	15.8	15.2	14.1	46%	22%	27%	3631	502	1427
2/3,4			17.65	20.1	19.3	18.0	46%	21%	29%	2872	362	740
1/12	14°	1	9.4	8.4	9.3	9.0	62%	31%	35%	1085	171	363
1/9			13.85	11.8	12.8	12.7	60%	29%	35%	2871	422	845
1/11			17.8	14.9	16.1	16.3	62%	27%	34%	2574	420	771
1/14	22°	1	9.3	2.6	5.5	7.5	140%	45%	48%	3057	237	128
2/8	18°		17.65	5.9	9.2	13.6	119%	52%	47%	4297	516	222
1/18	0°	2	9.3	10.5	9.9	9.3	51%	33%	32%	4113	693	1646
2/2			17.65	20.2	18.5	17.9	46%	25%	28%	2629	435	953
1/19	0°	3	9.3	9.5	9.3	8.7	50%	27%	30%	4303	704	1668
1/22		(edge)	17.65	19.1	17.5	16.8	48%	24%	28%	3629	652	1357
1/20	0°	4	9.3	8.6	8.5	7.9	56%	36%	35%	3533	620	1404
1/21		(corner)	17.65	14.5	14.6	13.7	54%	29%	36%	3385	558	1235
1/15	29°	5 (edge)	9.3	5.6	7.3	9.0	78%	37%	37%	3304	518	527

Table IX-2 Comparison of Three Analysis Methods

METHOD	Total No. of Events (6 runs)	$\frac{E_{Calculated} - E_{true}}{E_{true}}$ % average for 6 runs	σ% average for 6 runs
(1) All single, K = 3.71	17208	13%	54%
(2) Interaction in T12 or I1, K = 5.07	2465	7%	26%
(3) Interaction in T12, I1-I6 K=K(d,E) d >20 cm.	5992	5%	31%

List of Figures

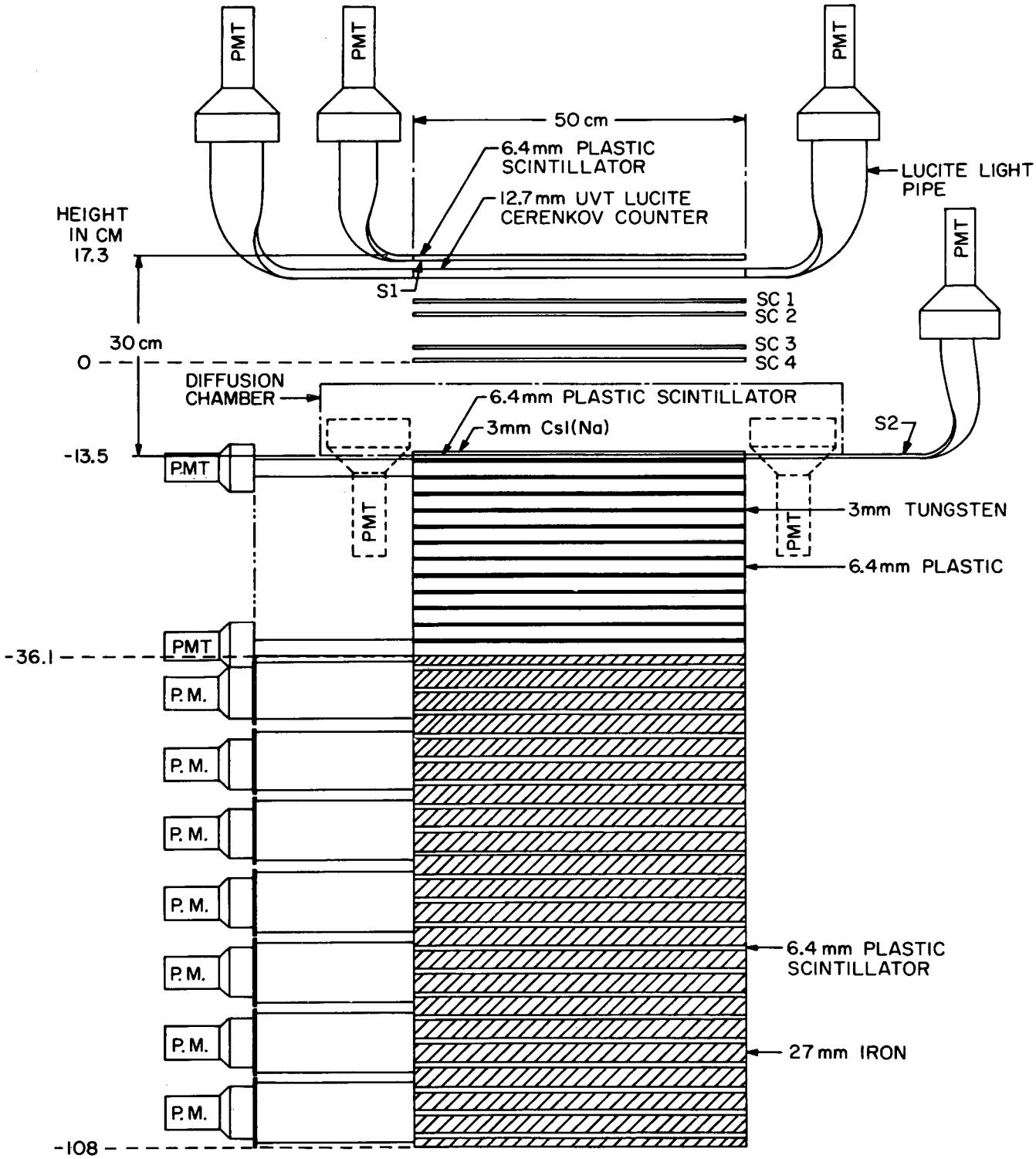

IONIZATION SPECTROMETER

Figure I-1

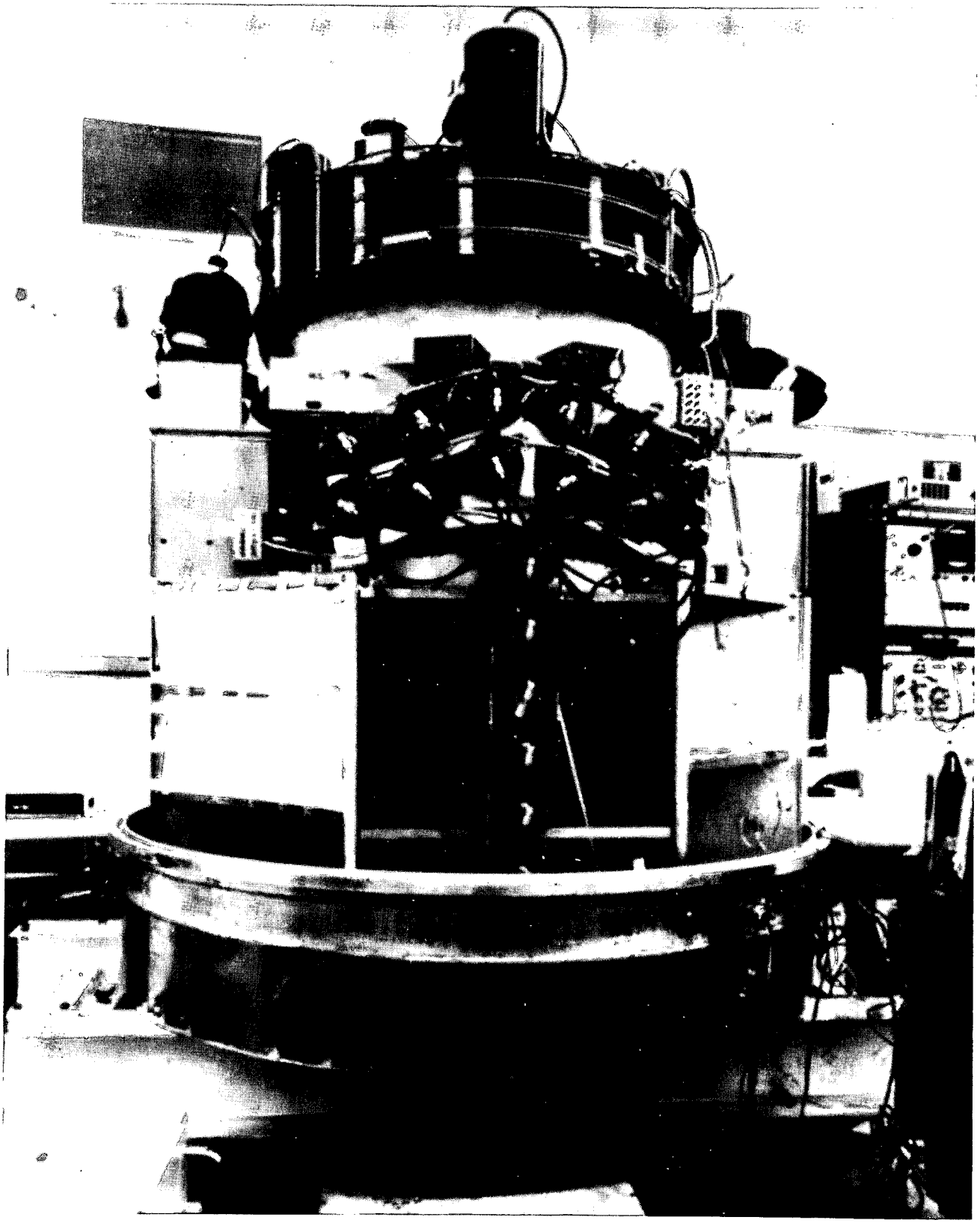

Figure I-2

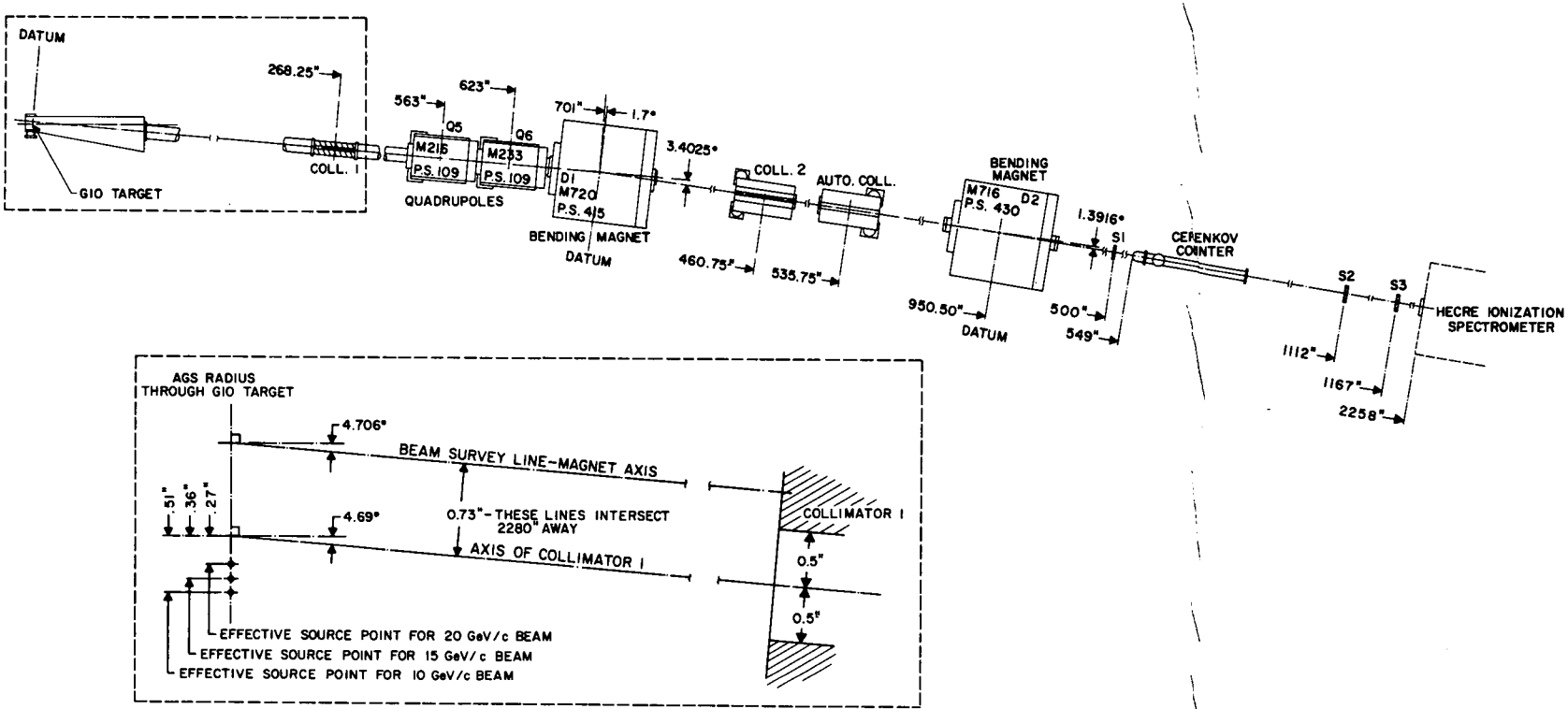

SCHEMATIC OF G-10 +4.7° TEST BEAM
TRANSPORT SYSTEM 18-21 JULY 1970

Figure II-1

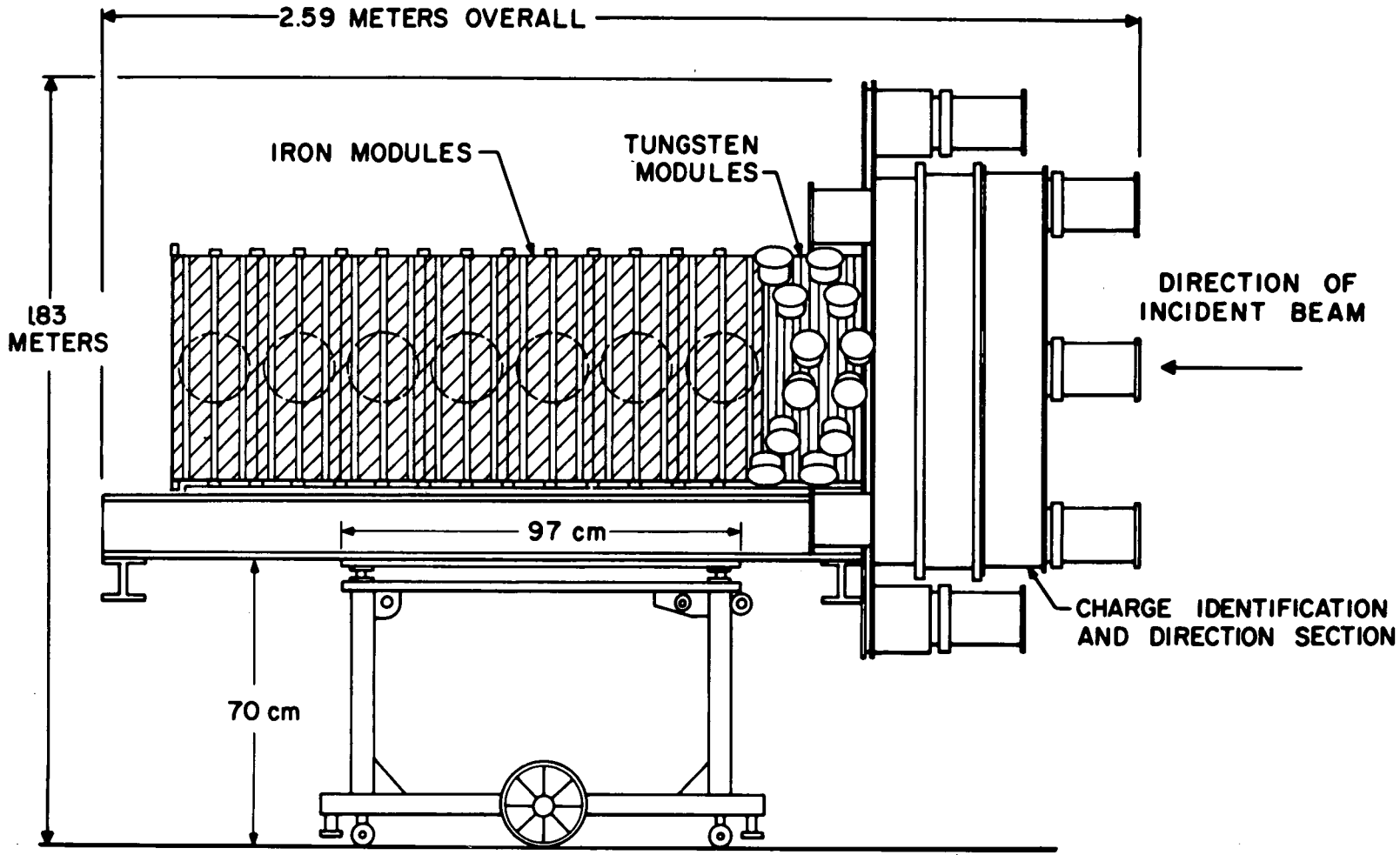

HIGH ENERGY COSMIC RAY EXPERIMENT

Figure II-2

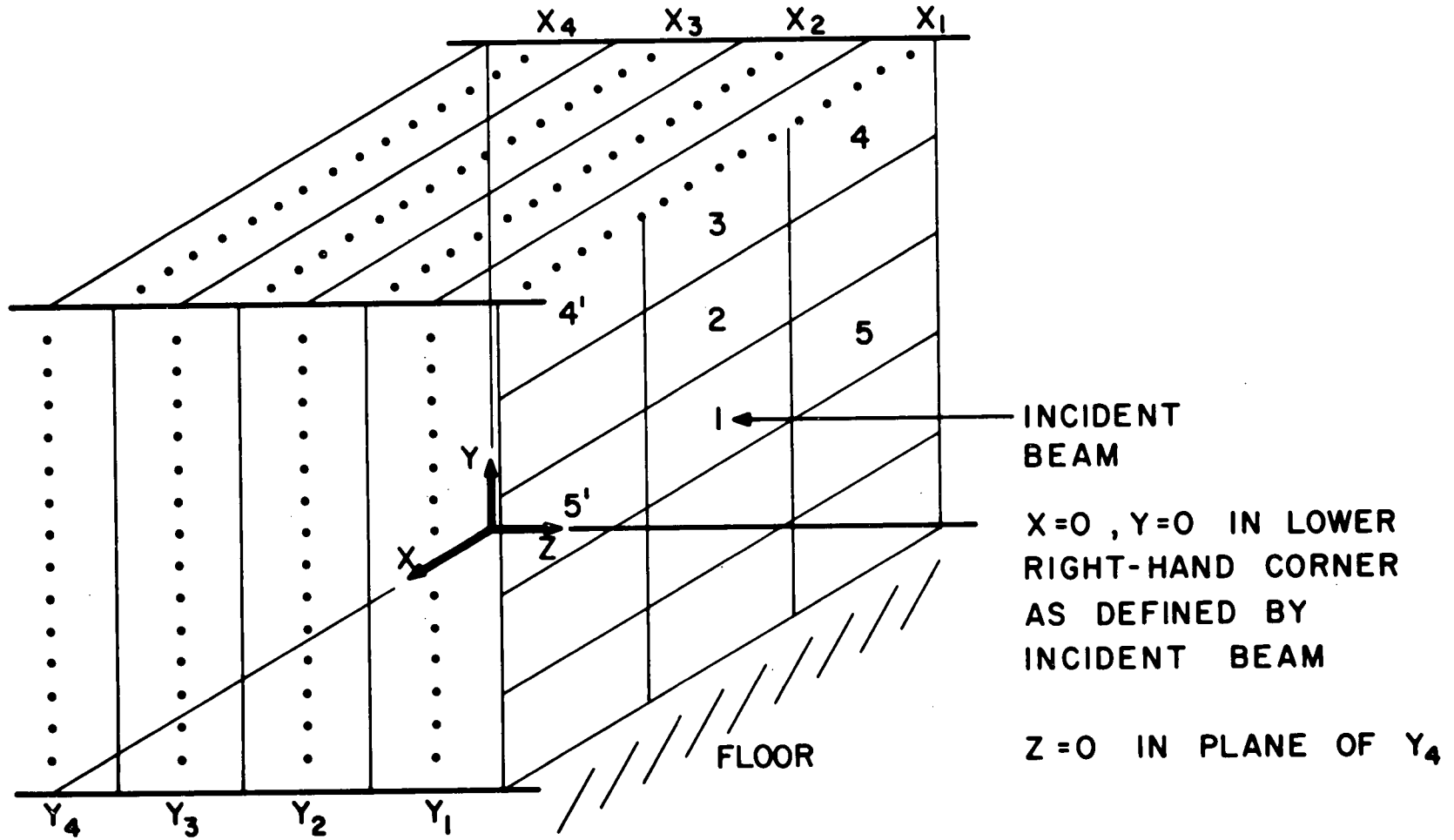

Figure II-3

SPARK CHAMBER ORIENTATION WITH RESPECT TO INCIDENT BEAM
DURING BNL CALIBRATION

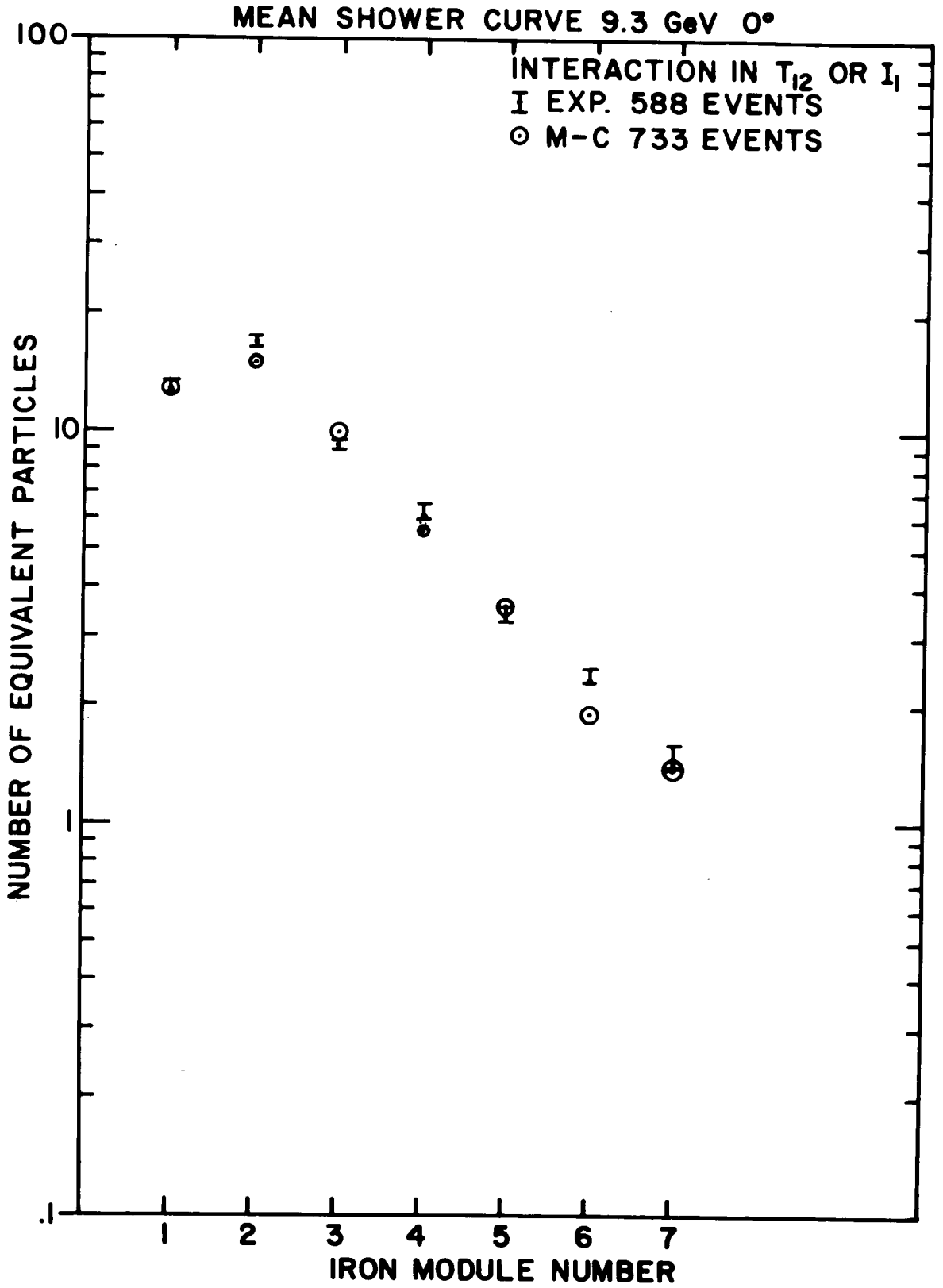
MEAN SHOWER CURVE 9.3 GeV 0°
INTERACTION IN T_{12} OR I_1
I EXP. 588 EVENTS
⊙ M-C 733 EVENTS
NUMBER OF EQUIVALENT PARTICLES
100
10
1
.1
1
2
3
4
5
6
7
IRON MODULE NUMBER

Figure III-1

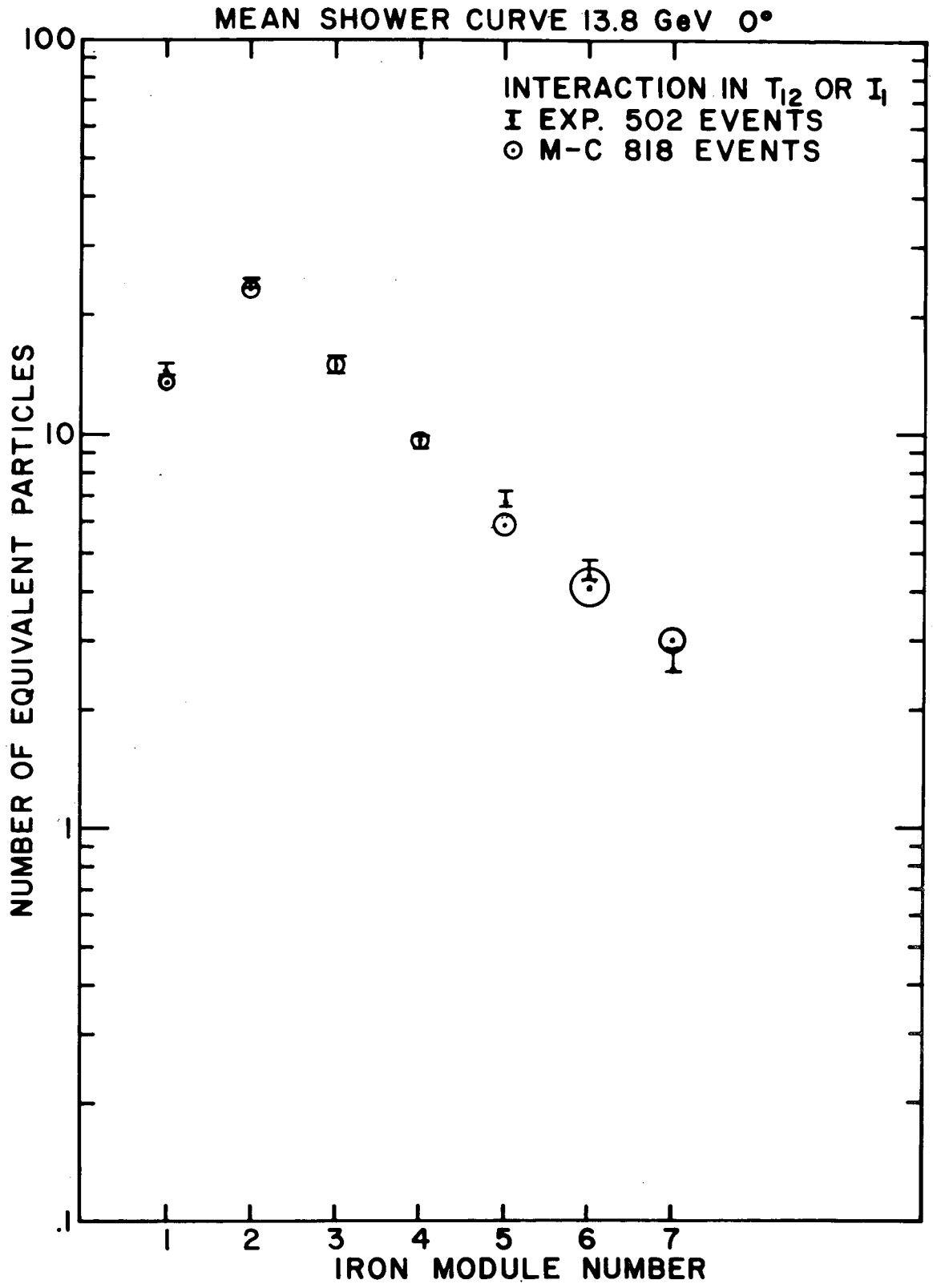
MEAN SHOWER CURVE 13.8 GeV 0°
INTERACTION IN T_{12} OR I_1
I EXP. 502 EVENTS
⊙ M-C 818 EVENTS
NUMBER OF EQUIVALENT PARTICLES
100
10
1
.1
1
2
3
4
5
6
7
IRON MODULE NUMBER

Figure III-2

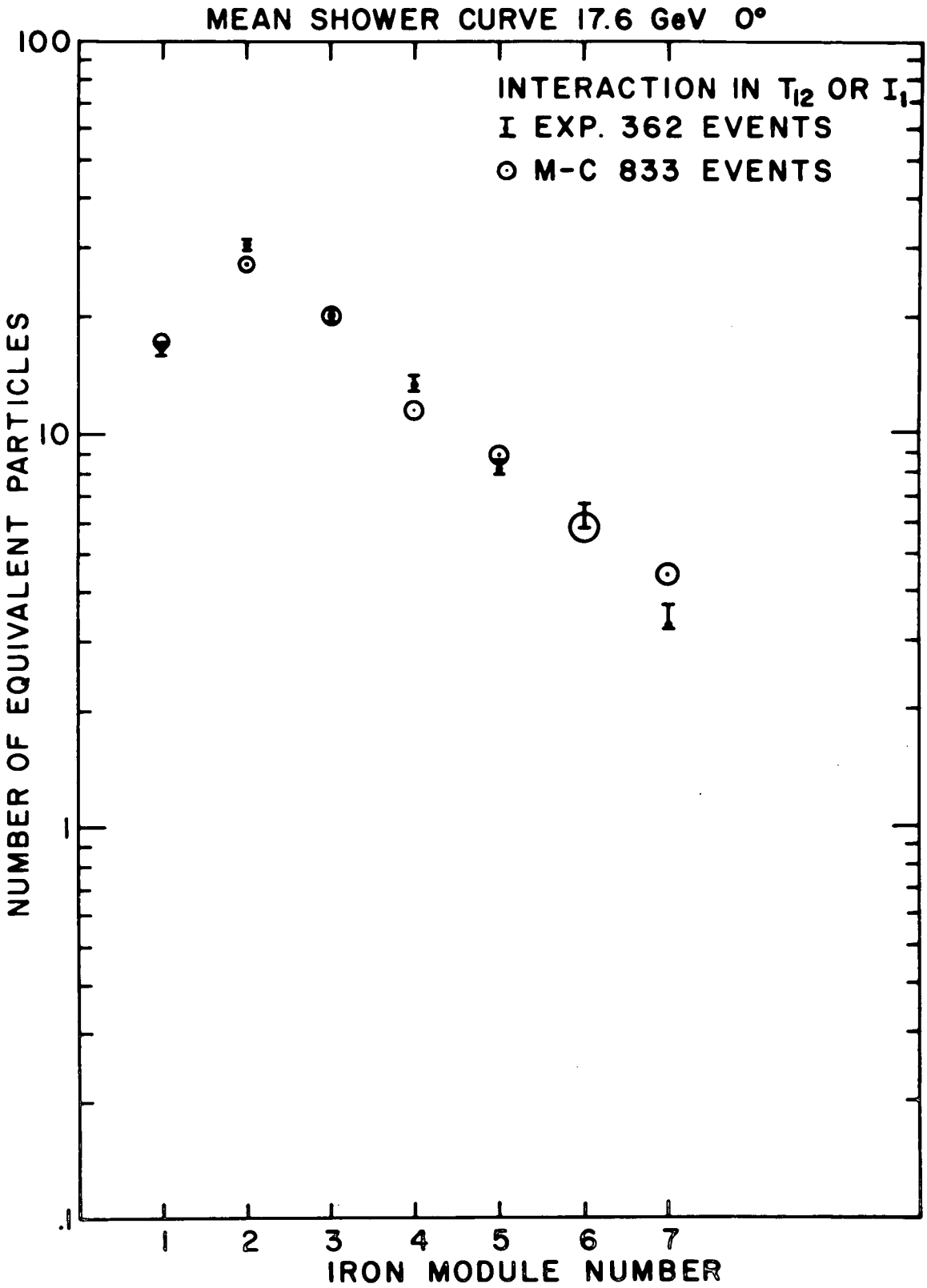
MEAN SHOWER CURVE 17.6 GeV 0°
INTERACTION IN T_{12} OR I_1
I EXP. 362 EVENTS
⊙ M-C 833 EVENTS
NUMBER OF EQUIVALENT PARTICLES
100
10
1
.1
1
2
3
4
5
6
7
IRON MODULE NUMBER

Figure III-3

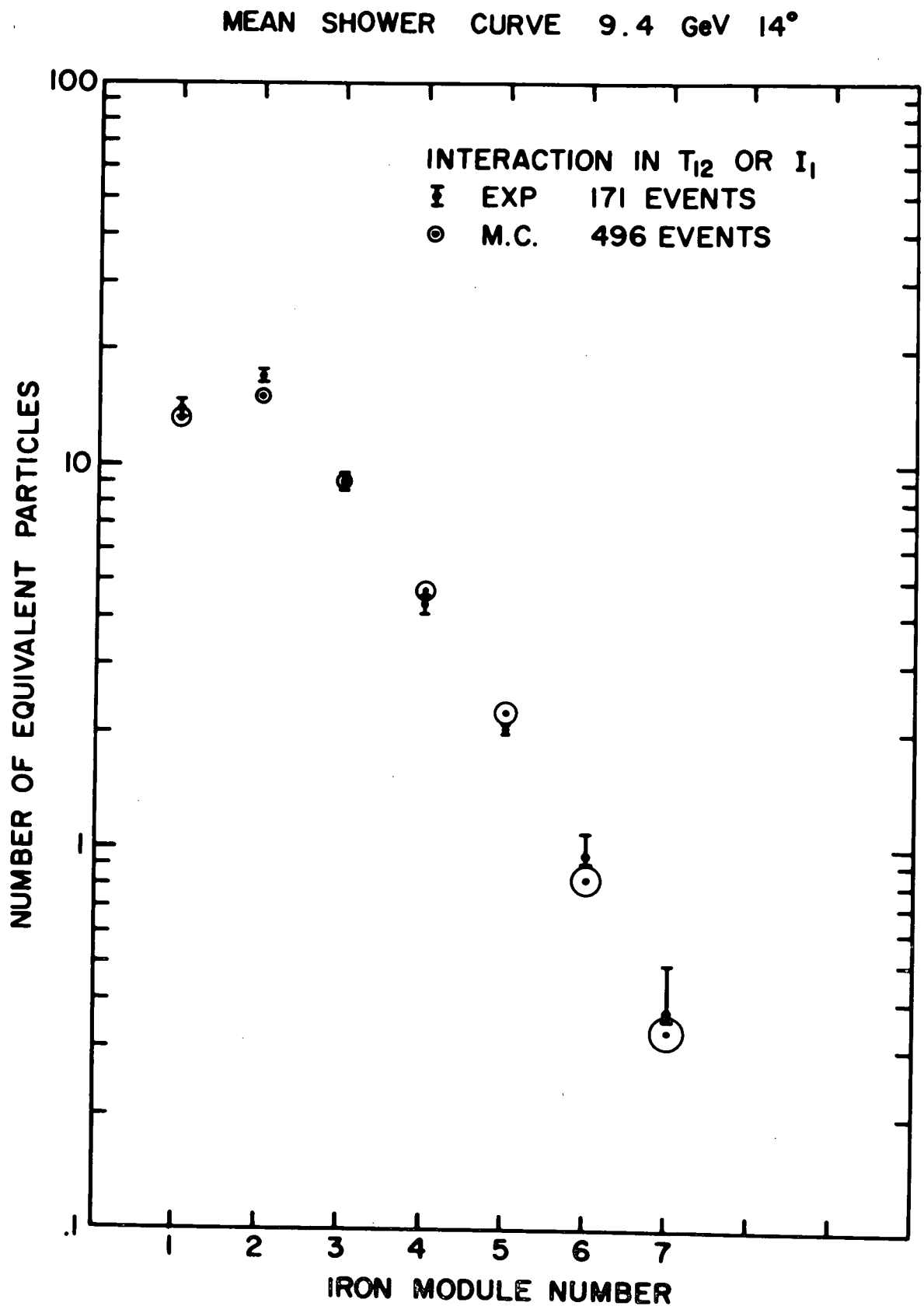
MEAN SHOWER CURVE 9.4 GeV 14°
INTERACTION IN T_{12} OR I_1
EXP 171 EVENTS
M.C. 496 EVENTS
NUMBER OF EQUIVALENT PARTICLES
100
10
1
.1
1
2
3
4
5
6
7
IRON MODULE NUMBER

Figure III-4

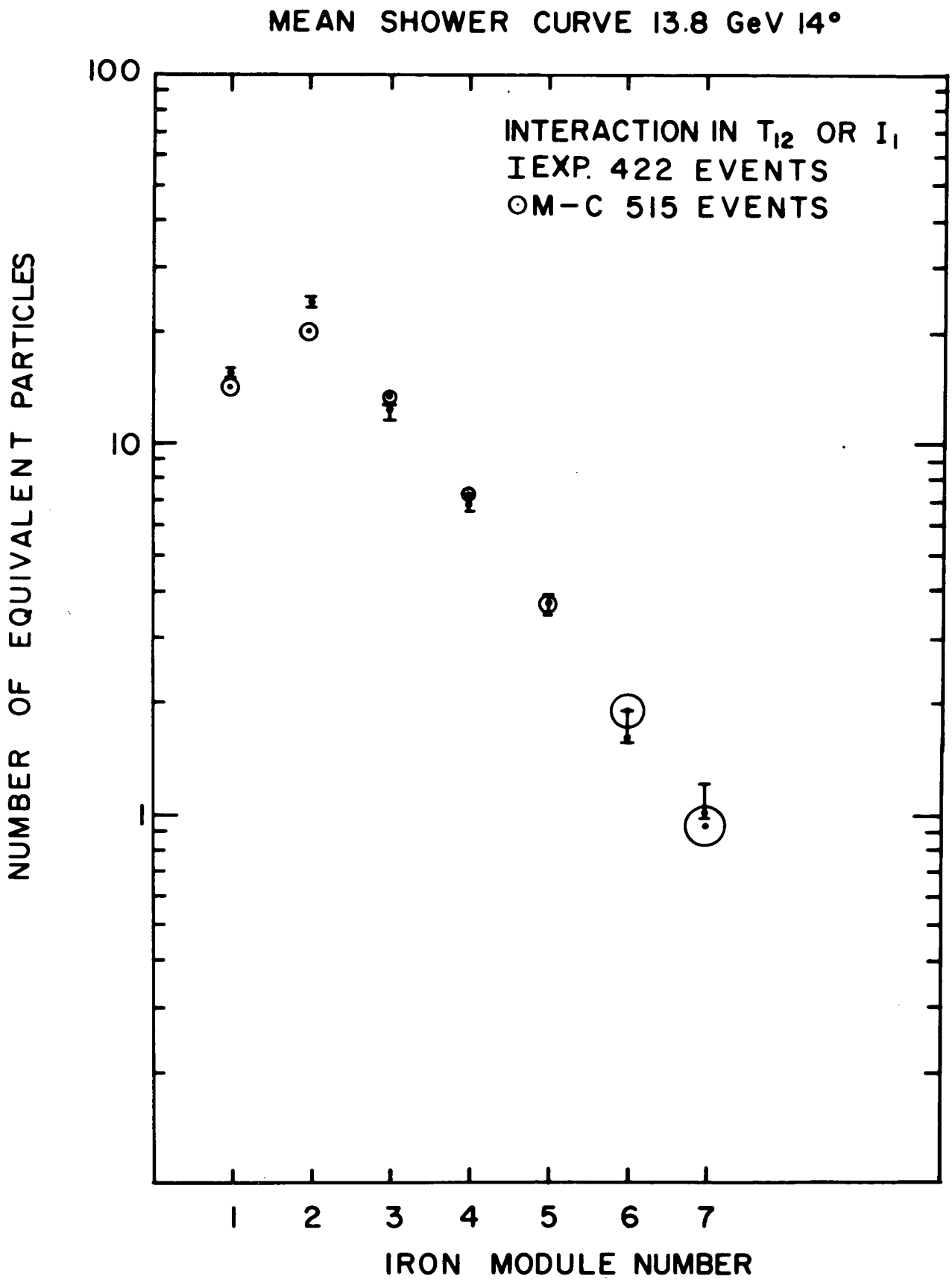
MEAN SHOWER CURVE 13.8 GeV 14°
INTERACTION IN T_{12} OR I_1
IEXP. 422 EVENTS
⊙M-C 515 EVENTS
NUMBER OF EQUIVALENT PARTICLES
100
10
1
1
2
3
4
5
6
7
IRON MODULE NUMBER

Figure III-5

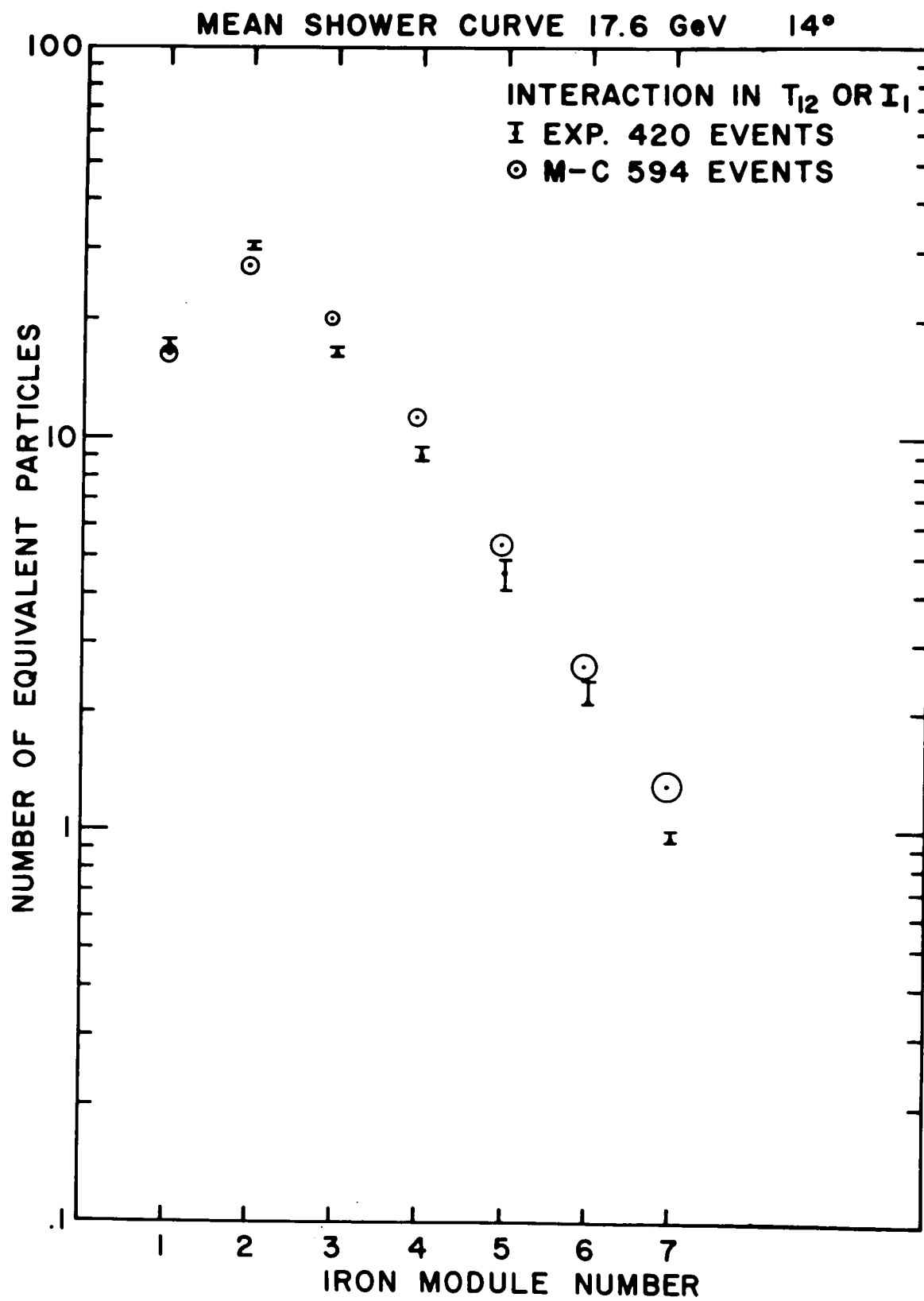
MEAN SHOWER CURVE 17.6 GeV 14°
INTERACTION IN T_{12} OR I_1
I EXP. 420 EVENTS
⊙ M-C 594 EVENTS
NUMBER OF EQUIVALENT PARTICLES
100
10
1
.1
1
2
3
4
5
6
7
IRON MODULE NUMBER

Figure III-6

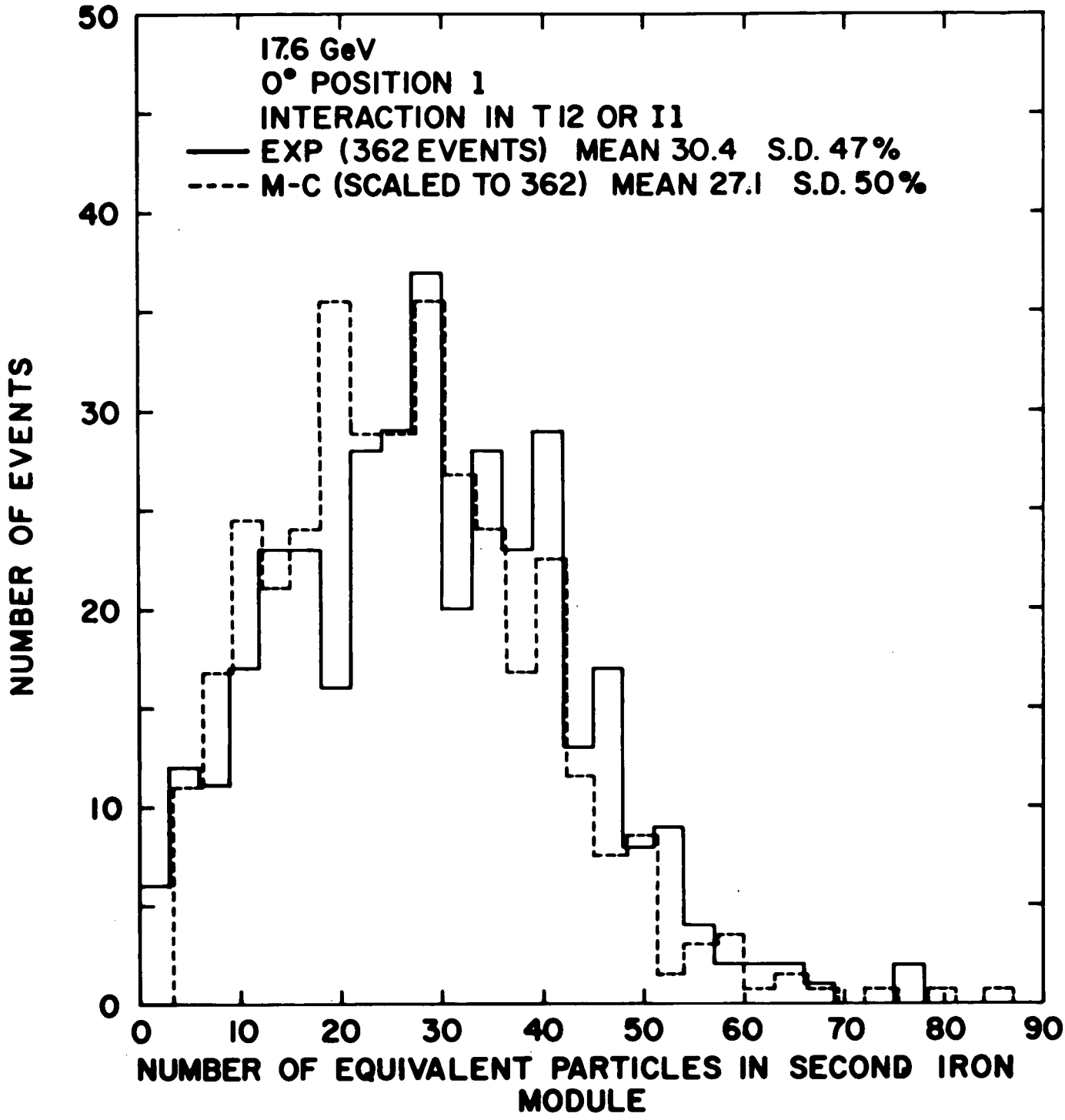
17.6 GeV
0° POSITION 1
INTERACTION IN T12 OR I1
EXP (362 EVENTS) MEAN 30.4 S.D. 47%
M-C (SCALED TO 362) MEAN 27.1 S.D. 50%
NUMBER OF EVENTS
0
10
20
30
40
50
0
10
20
30
40
50
60
70
80
90
NUMBER OF EQUIVALENT PARTICLES IN SECOND IRON MODULE

Figure III-7

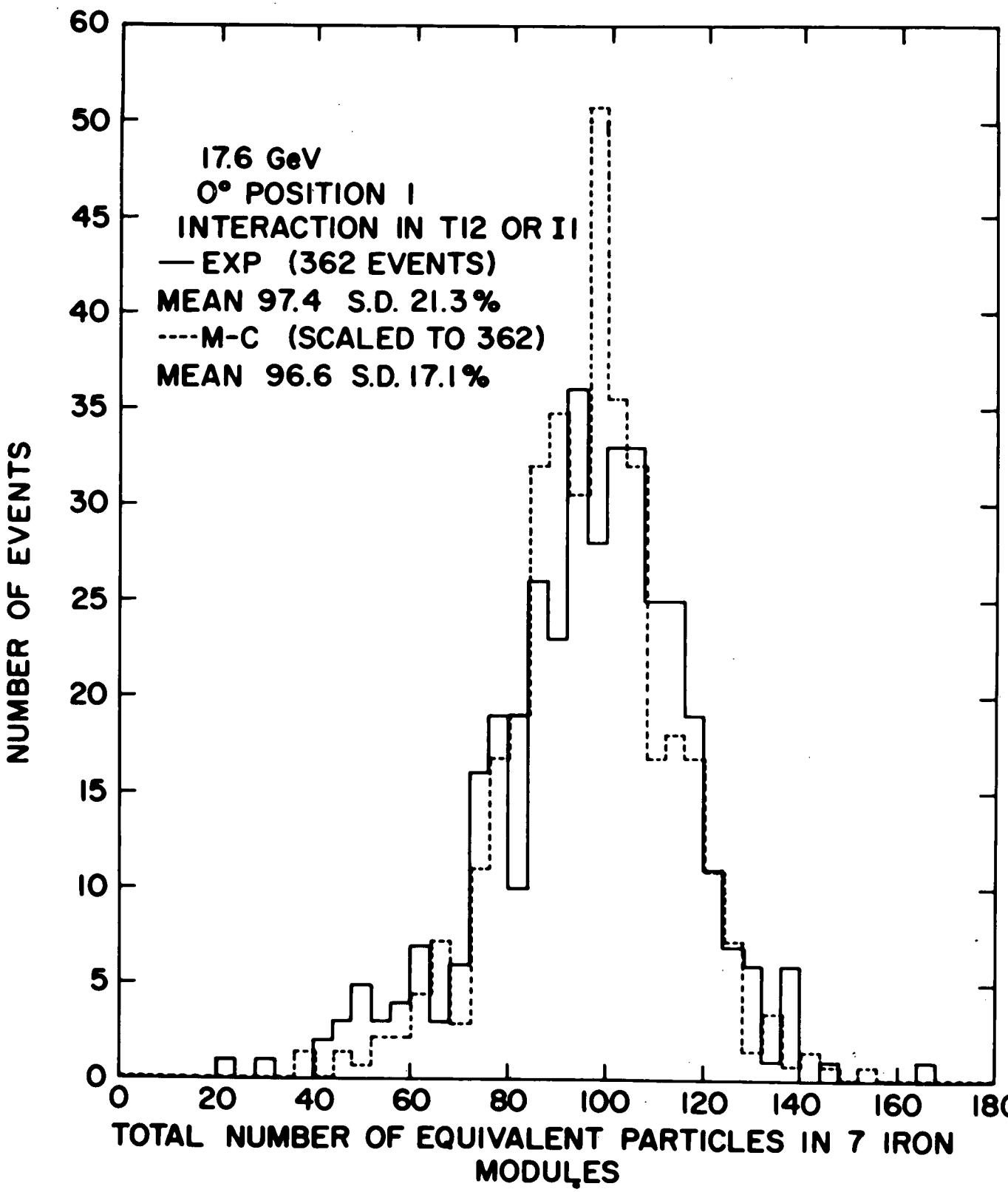
17.6 GeV
0° POSITION 1
INTERACTION IN T12 OR I1
— EXP (362 EVENTS)
MEAN 97.4 S.D. 21.3%
----M-C (SCALED TO 362)
MEAN 96.6 S.D. 17.1%
NUMBER OF EVENTS
0
5
10
15
20
25
30
35
40
45
50
60
0
20
40
60
80
100
120
140
160
180
TOTAL NUMBER OF EQUIVALENT PARTICLES IN 7 IRON MODULES

Figure III-8

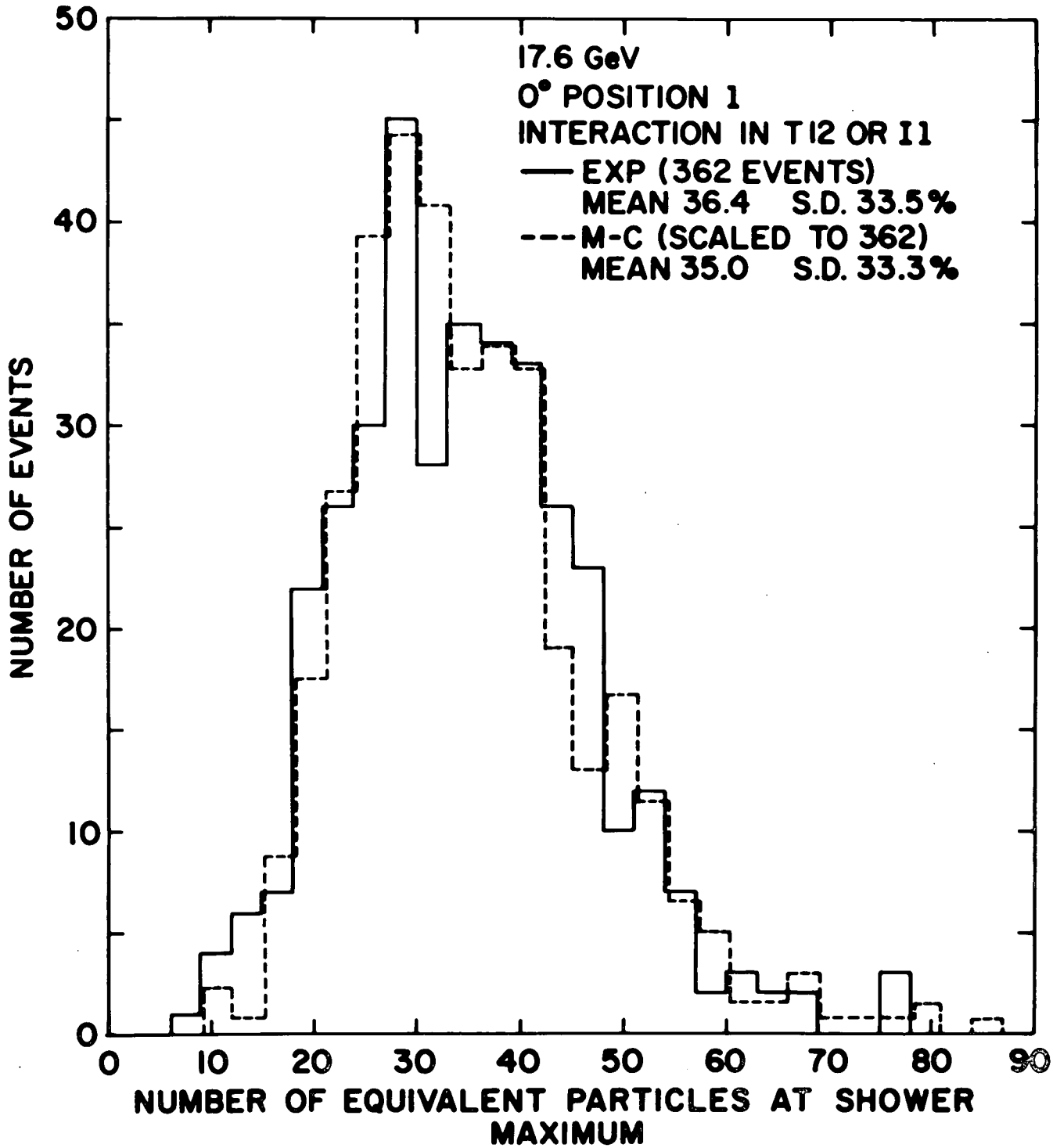
17.6 GeV
0° POSITION 1
INTERACTION IN T12 OR I1
EXP (362 EVENTS)
MEAN 36.4 S.D. 33.5%
M-C (SCALED TO 362)
MEAN 35.0 S.D. 33.3%
NUMBER OF EVENTS
0
10
20
30
40
50
60
70
80
90
NUMBER OF EQUIVALENT PARTICLES AT SHOWER MAXIMUM

Figure III-9

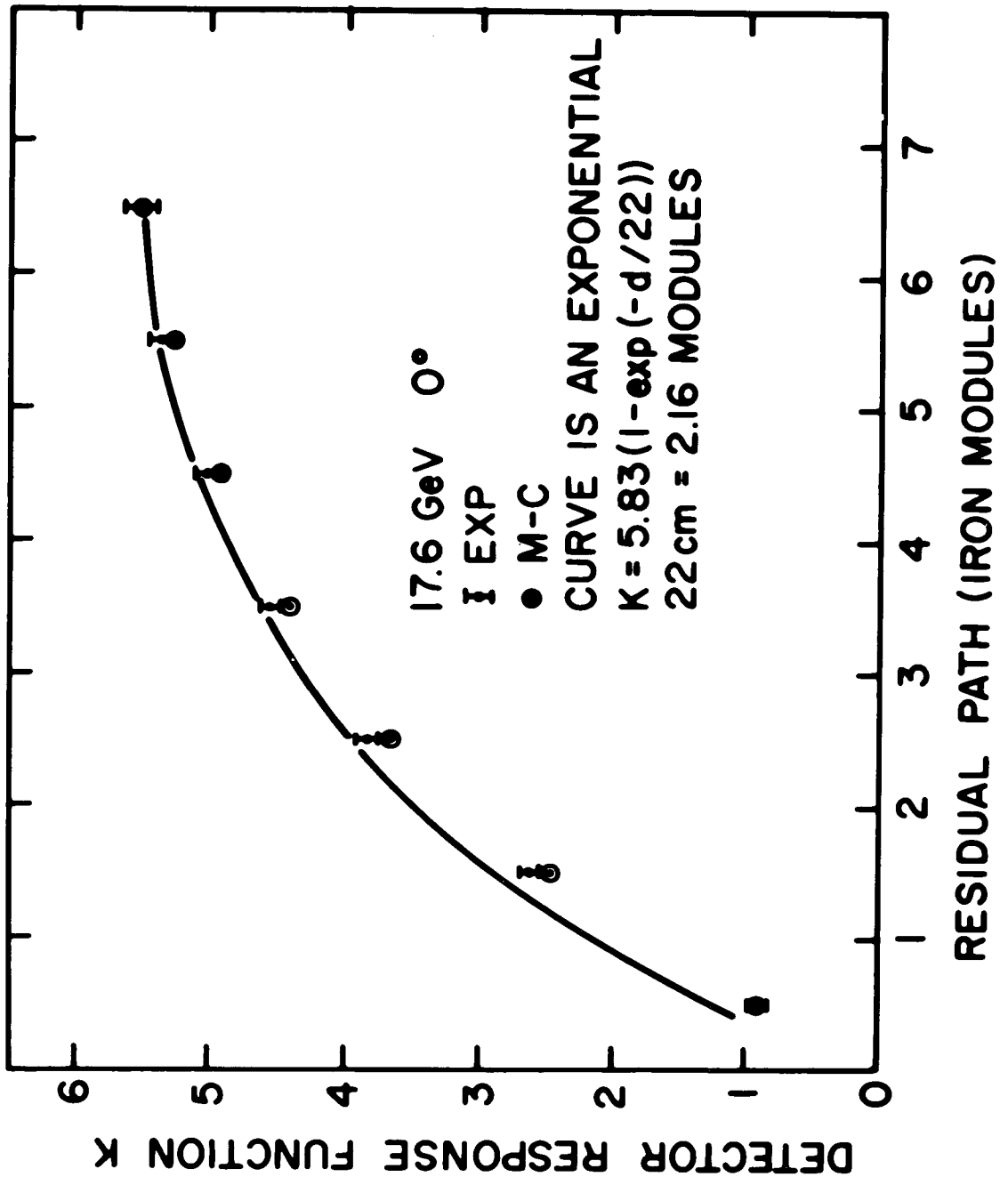
DETECTOR RESPONSE FUNCTION K
RESIDUAL PATH (IRON MODULES)
17.6 GeV 0°
I EXP
● M-C
CURVE IS AN EXPONENTIAL
K = 5.83(1-exp(-d/22))
22cm = 2.16 MODULES

Figure IV-1

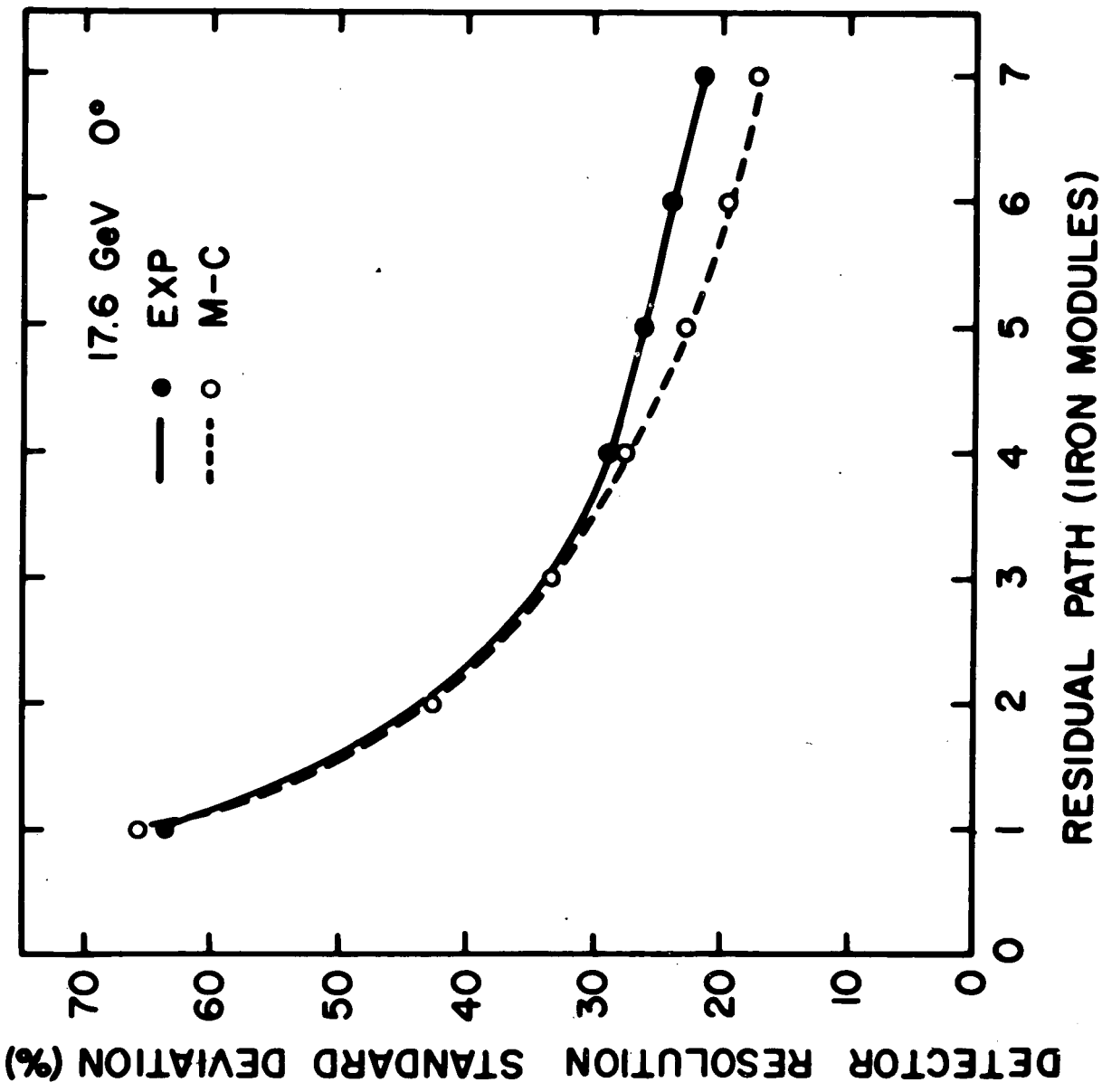
17.6 GeV 0°
EXP
M-C
RESIDUAL PATH (IRON MODULES)
0
1
2
3
4
5
6
7
DETECTOR RESOLUTION STANDARD DEVIATION (%)
0
10
20
30
40
50
60
70

Figure IV-2

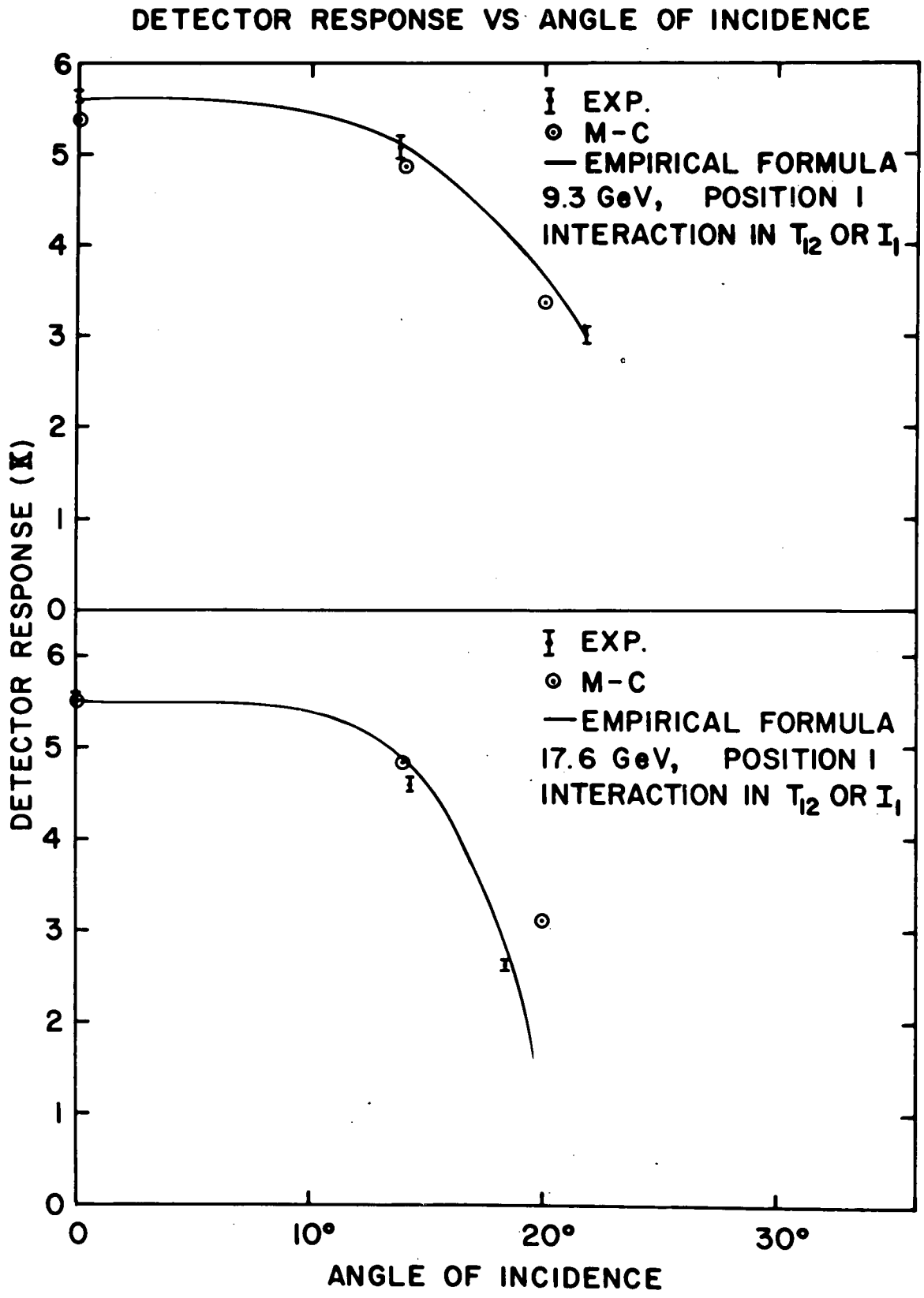
DETECTOR RESPONSE VS ANGLE OF INCIDENCE
I EXP.
⊙ M-C
— EMPIRICAL FORMULA
9.3 GeV, POSITION I
INTERACTION IN T_{12} OR I_1
I EXP.
⊙ M-C
— EMPIRICAL FORMULA
17.6 GeV, POSITION I
INTERACTION IN T_{12} OR I_1
DETECTOR RESPONSE (K)
0
1
2
3
4
5
6
0
10°
20°
30°
ANGLE OF INCIDENCE

Figure IV-3

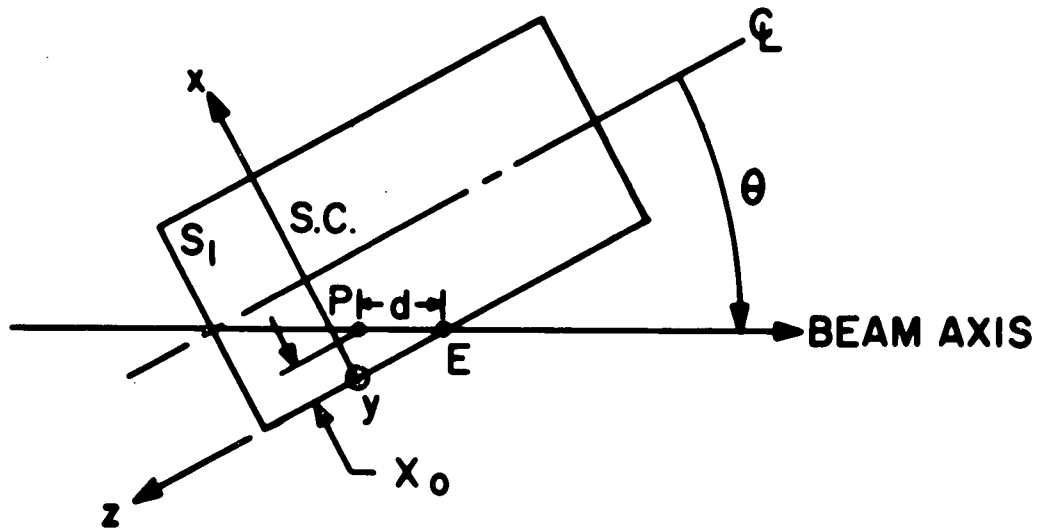

DETECTOR GEOMETRY FOR RESIDUAL PATH DETERMINATION

Figure IV-4

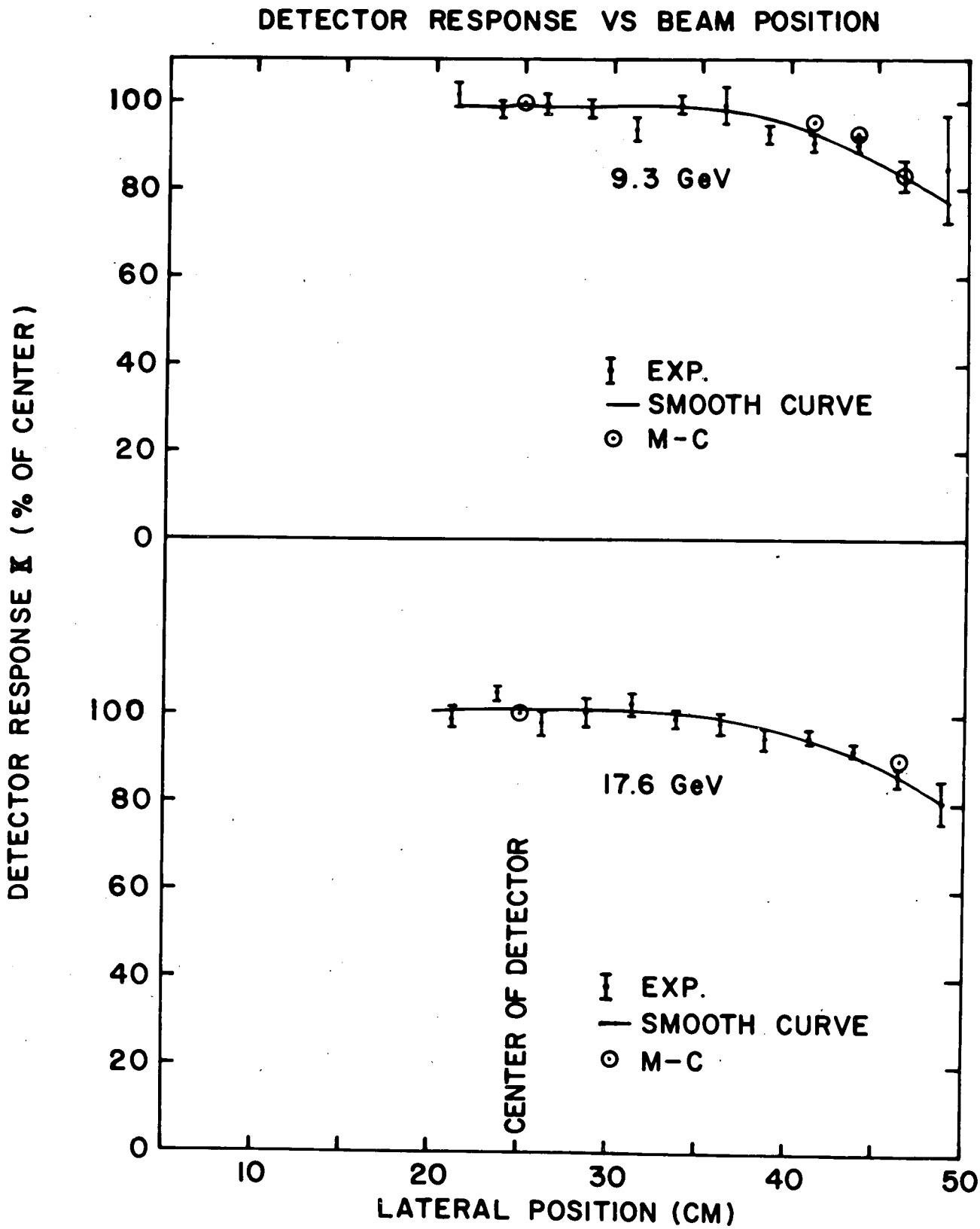
DETECTOR RESPONSE VS BEAM POSITION
DETECTOR RESPONSE R (% OF CENTER)
100
80
60
40
20
0
9.3 GeV
I EXP.
— SMOOTH CURVE
⊙ M-C
100
80
60
40
20
0
17.6 GeV
CENTER OF DETECTOR
I EXP.
— SMOOTH CURVE
⊙ M-C
10
20
30
40
50
LATERAL POSITION (CM)

Figure IV-5

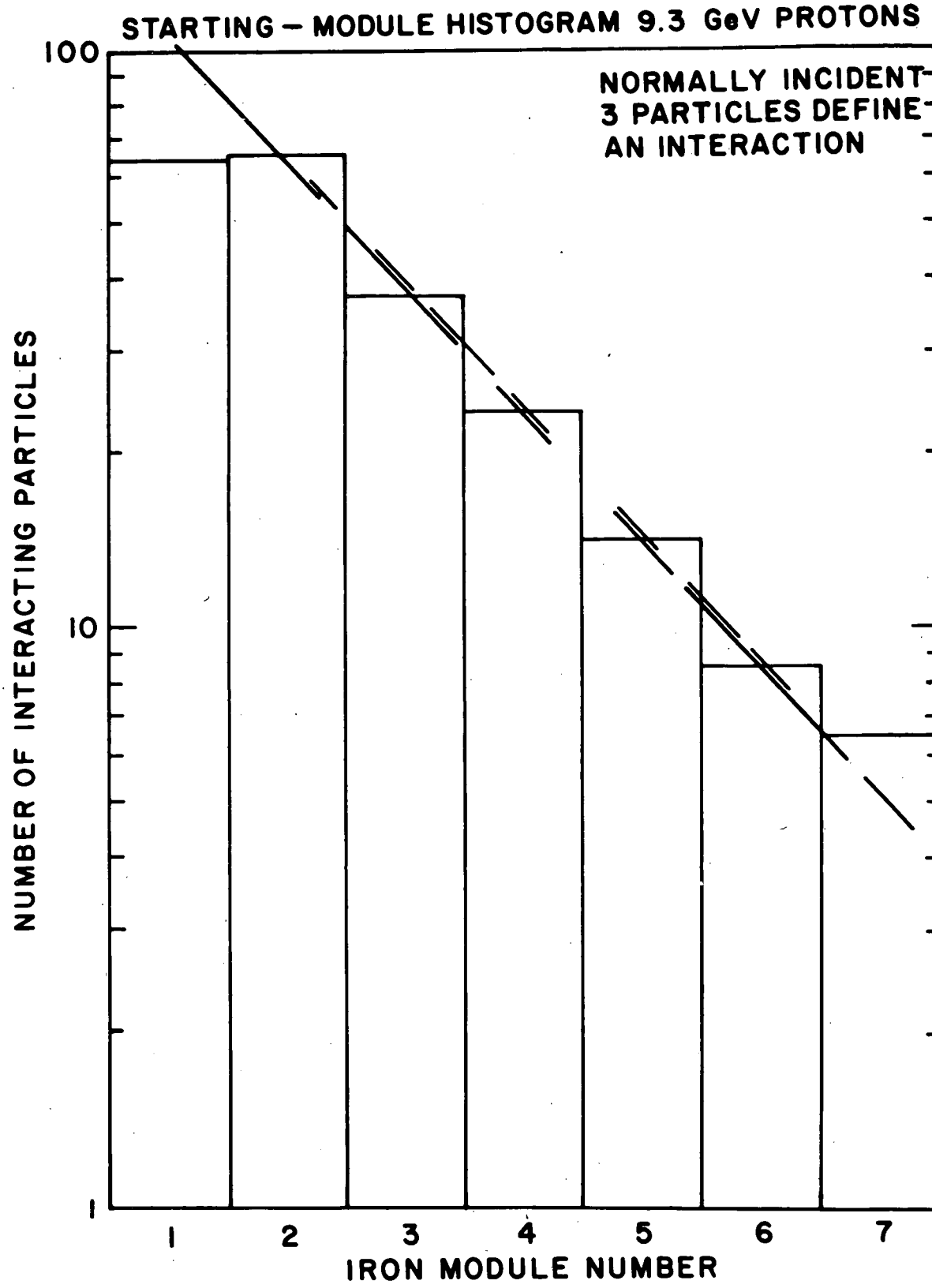
STARTING – MODULE HISTOGRAM 9.3 GeV PROTONS
NORMALLY INCIDENT
3 PARTICLES DEFINE
AN INTERACTION
100
10
1
NUMBER OF INTERACTING PARTICLES
1
2
3
4
5
6
7
IRON MODULE NUMBER

Figure VI-1

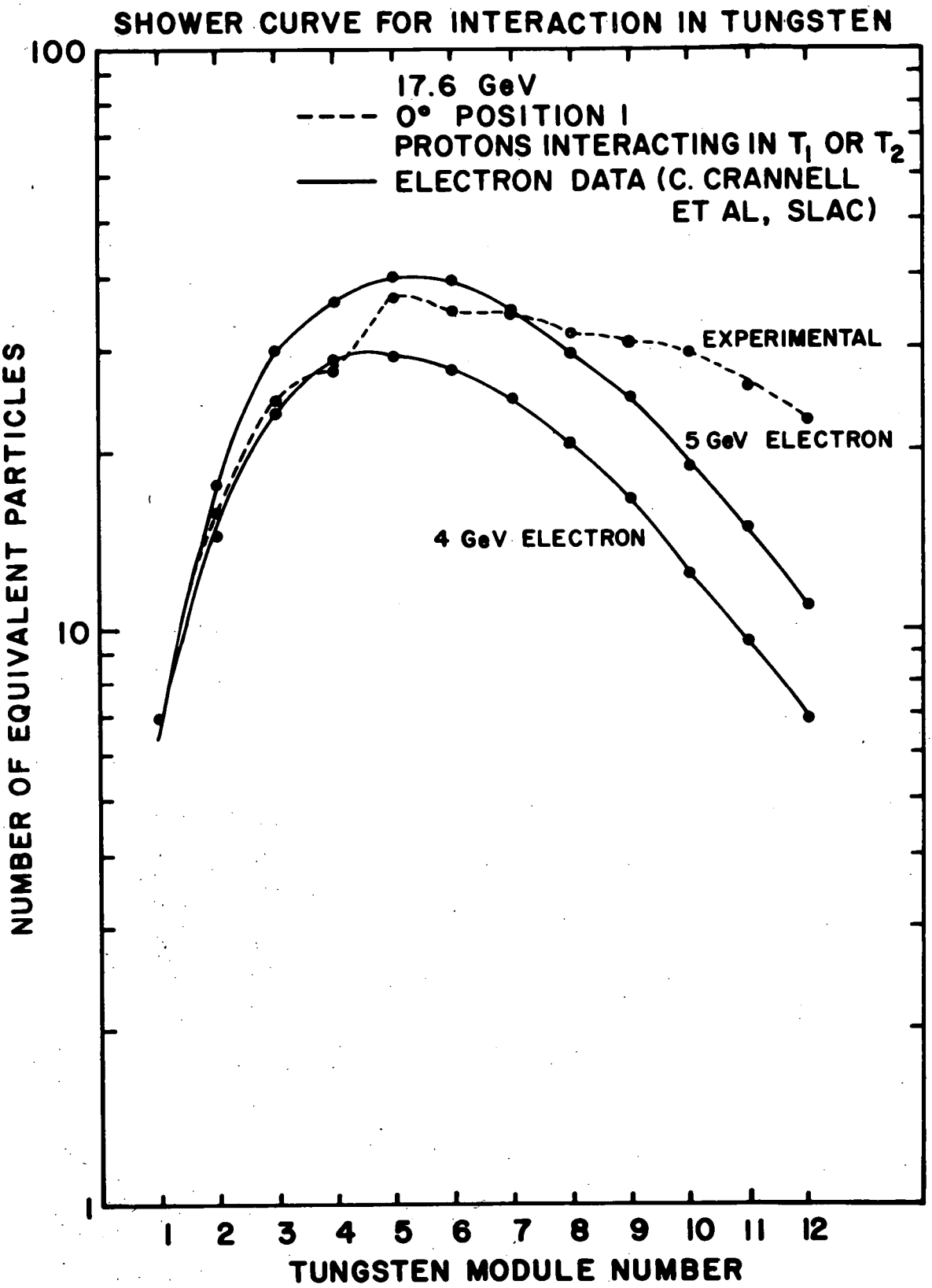
SHOWER CURVE FOR INTERACTION IN TUNGSTEN
17.6 GeV
0° POSITION I
PROTONS INTERACTING IN T1 OR T2
ELECTRON DATA (C. CRANNELL ET AL, SLAC)
EXPERIMENTAL
5 GeV ELECTRON
4 GeV ELECTRON
NUMBER OF EQUIVALENT PARTICLES
100
10
1
1 2 3 4 5 6 7 8 9 10 11 12
TUNGSTEN MODULE NUMBER

Figure VII-1

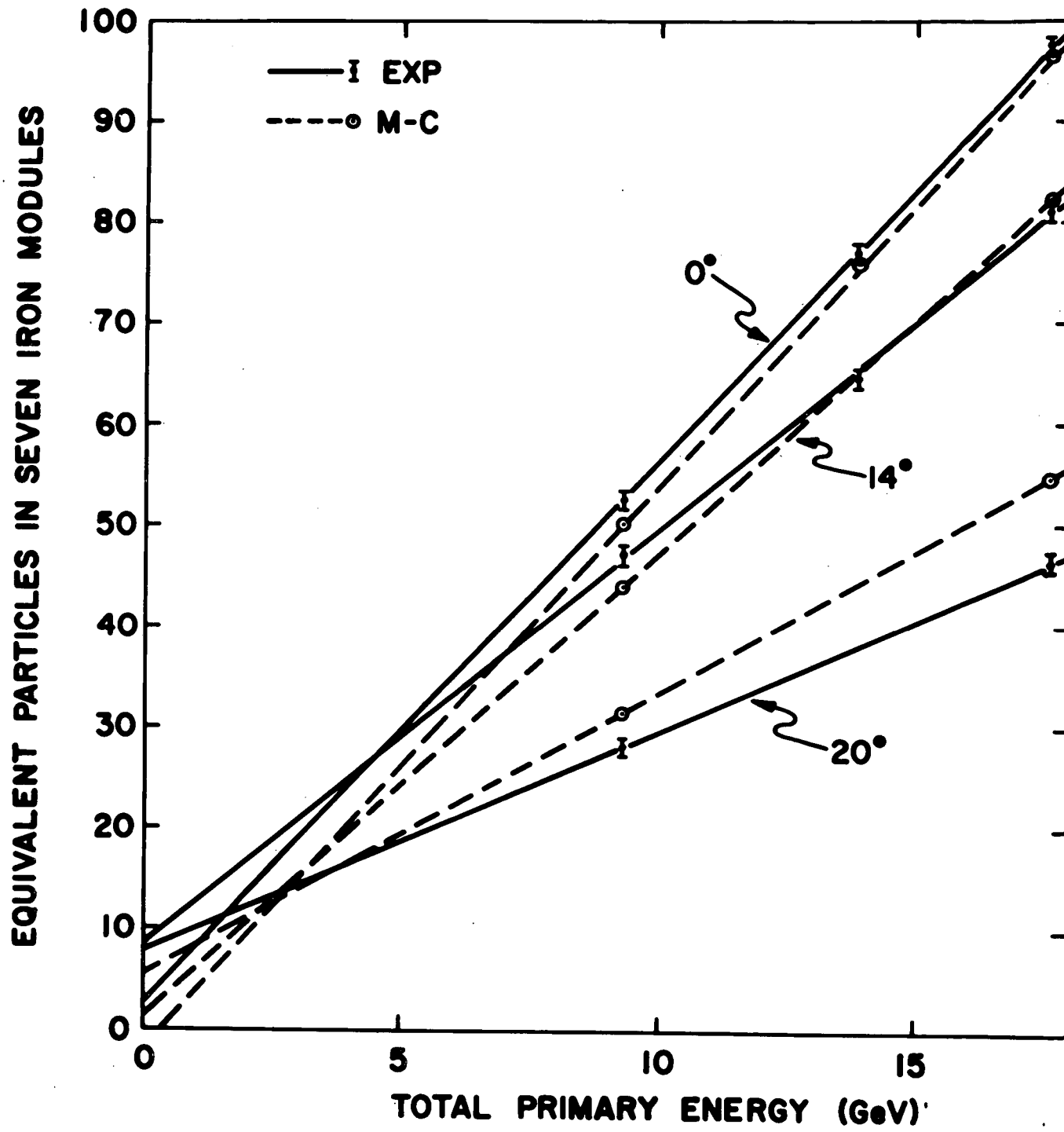

Figure VIII-1

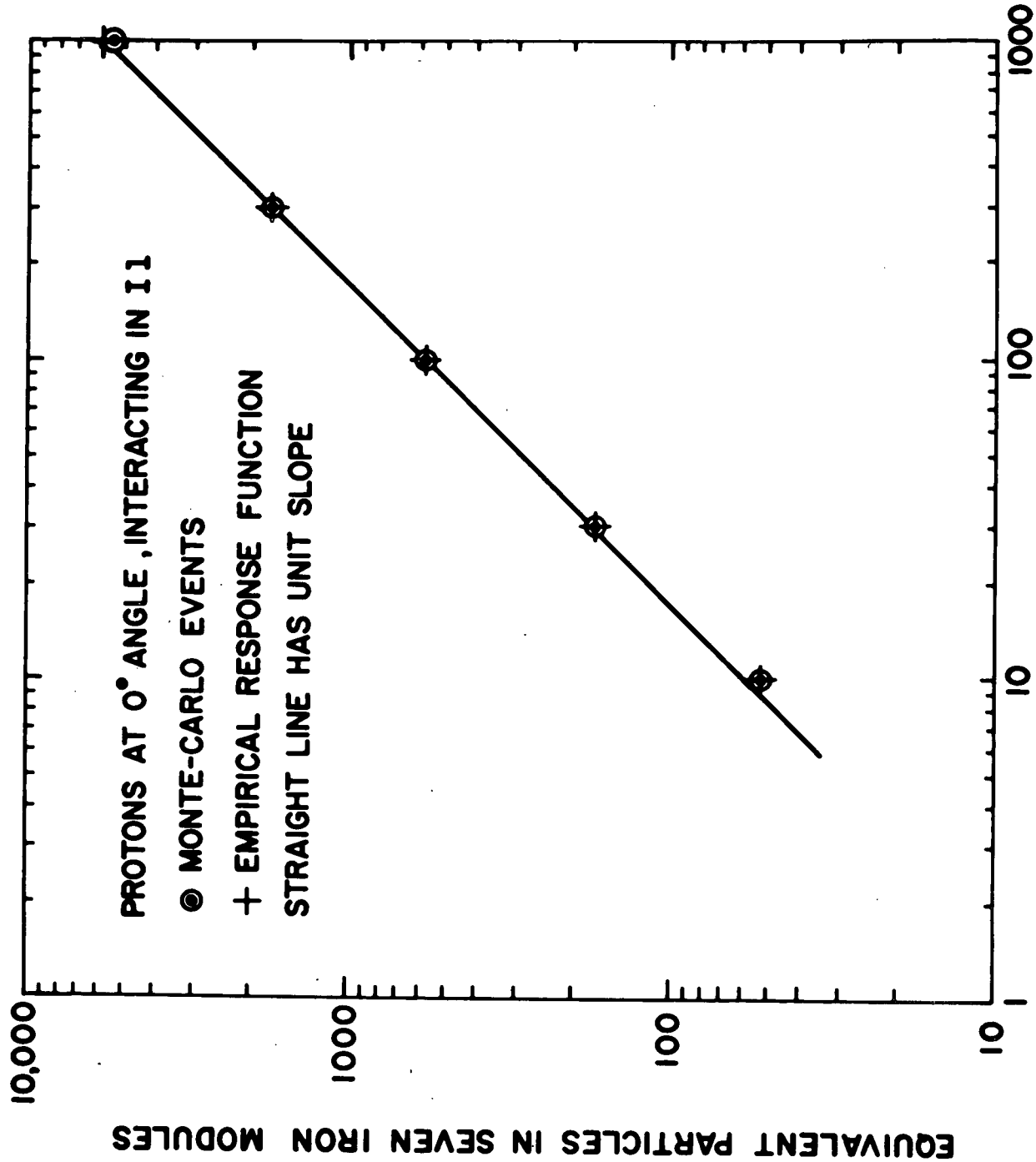

Figure VIII-2

* U.S. GOVERNMENT PRINTING OFFICE: 1972-735-961/7